

# **Local scale hydrodynamics and oxygen fluctuations near coral reefs**

A study of the relationship between hydrodynamics and dissolved oxygen near coral reefs around the island of Curaçao

Caitlin Holzhauser, Master of Marine Science  
Utrecht University  
30 June 2022

# Table of Contents

<b>SUMMARY</b> .....	<b>3</b>
<b>1. BACKGROUND/INTRODUCTION</b> .....	<b>4</b>
1.1 CURACAO AND ITS REEFS.....	4
1.2 CORAL SPECIES INTRODUCTION.....	4
1.3 BRIEF INTRODUCTION ON HYDRODYNAMICS.....	5
1.4 OXYGEN MECHANISMS OF CORAL REEFS.....	7
<b>2. OBJECTIVES AND PROBLEM DEFINITION</b> .....	<b>9</b>
2.1 RESEARCH QUESTIONS.....	10
2.1.1 <i>Sub question 1</i> .....	10
2.1.2 <i>Sub question 2</i> .....	10
2.1.3 <i>Sub question 3</i> .....	10
<b>3. METHODS</b> .....	<b>12</b>
3.1 LOCATION.....	12
3.2 AD2CP SETUP.....	13
3.3 MINIDOT SETUP.....	14
3.4 FIELDWORK.....	15
3.5 MODELLING.....	17
3.5.1 <i>Granger causality</i> .....	19
3.6 DATA ANALYSIS.....	20
3.6.1 <i>Current velocities</i> .....	20
3.6.2 <i>Wave data</i> .....	21
3.6.3 <i>Dissolved oxygen data</i> .....	21
<b>4. RESULTS</b> .....	<b>21</b>
4.1 RESULTS OF FIELDWORK.....	21
4.1.1 <i>Along shore</i> .....	21
4.1.2 <i>Cross-shore</i> .....	30
4.1.3 <i>Cross-shore vs along-shore</i> .....	37
4.1.4 <i>Statistical analysis</i> .....	45
4.2 MODEL FINDINGS.....	47
<b>5. DISCUSSION AND FUTURE RESEARCH</b> .....	<b>58</b>
5.1 RQ 1: ARE WAVES AND CURRENTS MEASURABLY DIFFERENT AROUND THE ISLAND?.....	58
5.2 RQ 2: CAN THE FOUND DIFFERENCES IN WAVES AND CURRENTS BE USED TO PREDICT THE LEVEL OF DISSOLVED OXYGEN NEAR CORAL REEFS?.....	59
5.3 RQ 3: WHAT CAN NUMERICAL MODELS TEACH US ABOUT THE IMPACT OF WATER FLOW ON DISSOLVED OXYGEN FLUCTUATIONS?.....	60
5.4 FUTURE RESEARCH.....	61
<b>REFERENCES</b> .....	<b>62</b>
<b>APPENDIX A – AD2CP DEPLOYMENT PLANS</b> .....	<b>67</b>
<b>APPENDIX B – MODEL METADATA</b> .....	<b>71</b>
<b>APPENDIX B.1 – TIME-INTERPOLATED VELOCITY</b> .....	<b>72</b>
<b>ACKNOWLEDGEMENTS</b> .....	<b>73</b>

## Summary

Coral reefs are a vital part of Curaçao's economy, providing revenue from ecotourism and fisheries, as well as providing shoreline protection. A vital coral species, *Diploria strigosa*, is a major reef-building species around the island, and contributes enormously to the health of the reefs, making it a prime candidate for this project. Physical oceanic processes, such as waves and currents, influence the health of these corals by introducing oxygen-rich water through mixing of the water column. In order to understand more about the growth and vitality of coral around Curaçao, it is therefore critical to understand how these processes influence the movement of oxygen around coral reefs.

This thesis set out to collect field data to investigate the existence of a relationship between hydrodynamics and dissolved oxygen near coral reefs around the island of Curaçao, as part of a larger project, the SEALINK project. SEALINK, part of the Dutch Research Council (NWO)'s Caribbean Research program, is an interdisciplinary research initiative to assess the impact of land-based and water-borne substances on the coral reefs of the Dutch Caribbean. Through a fieldwork campaign, dissolved oxygen concentration, wave data, and current velocity data was collected from seven study sites on the southern coast of Curaçao. Acoustic Doppler current profilers (AD2CP) and oxygen loggers were deployed through diving, and left on the seafloor to measure for six hours. A statistical analysis was run to test the validity of using current velocities as a predictor for dissolved oxygen values. Finally, a computational fluid dynamics (CFD) model was created using the fieldwork data in order to assist in the understanding of processes that influence dissolved oxygen around coral reefs. The results from fieldwork show that the extent of the relationship between waves, currents, and dissolved oxygen depends greatly on the location and tidal cycle. Study sites closer to the eastern point of the island showed that velocity and dissolved oxygen are connected, and that velocity has a greater capacity to predict dissolved oxygen values. The CFD model assists in a deeper comprehension of the influence of flow and other processes that can impact dissolved oxygen fluctuations around coral reefs.

# 1. Background/Introduction

## 1.1 Curaçao and its reefs

Tropical coral reefs cover less than 1% of the ocean floor globally, but are some of the most diverse and productive ecosystems in the world. Tropical reefs are home to a vast amount of reef fish and other marine organisms (Sandin et al., 2010). The reefs of Curaçao, first formed over 50 million years ago (de Bakker et al., 2016), are some of the healthiest reefs in the Caribbean, and despite their decline since the 1980s, host a higher number of fish compared to other Caribbean reefs. Coral reefs provide an important source of income for Curaçao through tourism and fishing, as well as provide protection from storm surges and flooding (Waitt Institute, 2017).

While there are many species of coral that exist around the island of Curaçao (Veron, 2000), a brain coral species, *Diploria strigosa* (hereafter referred to as *D. strigosa*), is most prominent all along the southern coast (i.e. the leeward side). We have limited the data collection to the southern coast because the northern coast (i.e. the windward side) of Curaçao is more volatile and rougher due to the existence of large cliffs and waves. *D. strigosa* is a reef-building species which is vital to the success of the reef system, and has been prolific around Curaçao since the 1980s (Waitt Institute, 2017). This makes the species a prime candidate for the research of this project.

## 1.2 Coral species introduction

An abundance of reef-building species is a good indicator of a healthy reef system (Waitt Institute, 2017). *D. strigosa*, a scleractinian (hard or stony) coral, is a major reef-building species in the Caribbean (Badgley et al., 2006). *D. strigosa* is found in depths ranging from 1-30 meters, growing at a rate of 3.3 mm per year, depending on water quality and temperature fluctuations (Harriot, 1999). Since 1973, there has been a steady decline in coral coverage around Curaçao (de Bakker et al, 2016), however, the decline of *D. strigosa* has been slow, with a shift towards a larger abundance of smaller growth forms. *D. strigosa* is a phenotypically plastic species, meaning that it exhibits different phenotypes in different

environmental settings. This may be one of the reasons *D. strigosa* is still seen all around the island, despite a slow decrease in colony size (de Bakker et al., 2016). Most work on hydrodynamics and coral reef has focused on branching corals (Asher et al., 2016; Green et al., 2018), with few studies done on brain corals and smooth-shaped hard coral (Monismith, 2007).

### 1.3 Brief introduction on hydrodynamics

The study of the movement of fluids, also known as hydrodynamics, is vital to the understanding of underwater ecosystems (Stocking et al., 2018; van Rooijen et al., 2020; Boudier et al., 2022). It is well known that physical oceanic processes, such as currents, internal and surface waves, upwelling and downwelling, and the tides influence the growth and health of coral reefs around the world (Monismith, 2007; Lowe et al., 2005). These processes can introduce colder, more nutrient-rich water to shallow water areas, and oxygenate the surface via mixing, making the shallow water where coral reefs thrive extremely habitable (Lowe et al., 2005). Leichter et al. (2005) found that internal waves - waves that are produced in deeper, density-stratified layers of the ocean - were responsible for transport of nutrients towards coral reef colonies in shallow water. This points towards the connection of ocean and biological processes.

Waves are one of the principal generators of circulation in shallow reef systems (Lowe et al., 2008); however, they can also be harmful and cause destruction, or decrease nutrient flow to and from reefs during periods of low to no waves (De'ath et al. 2012; Crabbe et al., 2008). Reidenbach et al. (2006) found that flow around a coral colony is increased when large waves (higher than usually present) occur. This means that

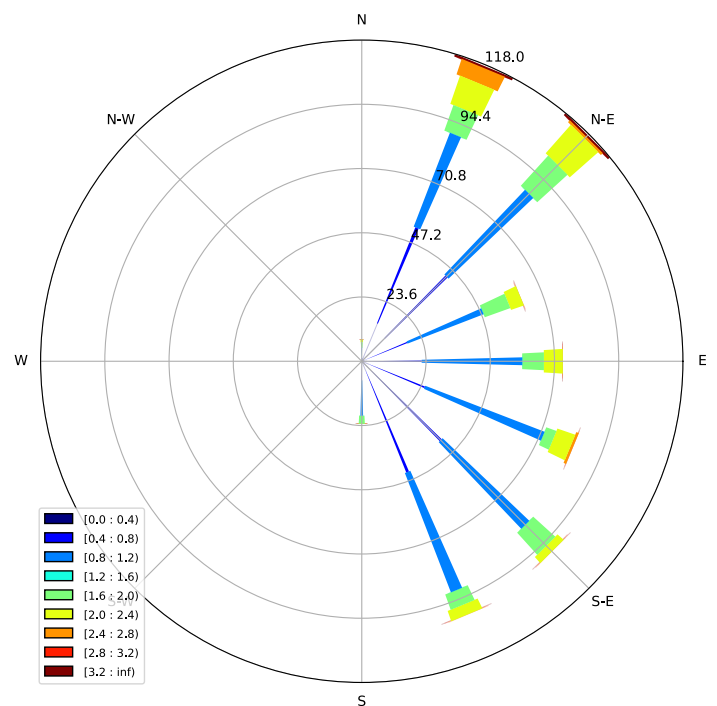


Figure 1: Wind speed and direction, Curaçao March 2022. The compass directions show which direction the wind is blowing. Speed is separated into ranges, seen in the legend on the bottom left.

shallow water corals are exposed to a high variation in surface waves (wave height and period primarily), potentially leading to a high rate of mass transfer of nutrients (Monismith, 2007). Around Curaçao, north-easterly winds are dominant, producing winddriven waves characterized by short duration and height (Meteorological Department Curaçao, 2022). The wind speeds and directions for the month of March 2022 (the study period) are shown in figure 1. Coral reefs have further been found to protect nearby shores by attenuating wind-induced storm surges by dissipating wave energy onto the reef flat (van Rooijen et al., 2020).

Tidal cycles and ranges can also influence the amount of mixing and water flow on island scales. Tidal fluctuations, driven by the gravitational pull of the moon and the rotation of the earth, can be diurnal (one high and low tide per day) or semidiurnal (two high and low tides per day), as shown in figure 2. These period cycles of the tide depend on the cycle of the moon (Cordier et al., 2013). Spring tides, or king tides, occur during full moons and result in high tides that are larger than average, and low tides that are lower than average. This period of larger tidal ranges occurs twice a month, with neap tides occurring in between. Neap tides result in smaller tidal ranges, when high tide and low tide are close in height (US Department of Commerce, 2014).

Tidal cycle influences the height of waves by controlling the sea surface height, and also creates currents, called tidal currents, in shallow water areas such as coastal areas (Becker et al. 2014). These currents are the dominant force in shallow waters. As the tide changes, the energy of incoming waves and currents can also change, increasing or decreasing as the water level decreases or rises (Monismith, 2007). Strong tidal currents can transport nutrients

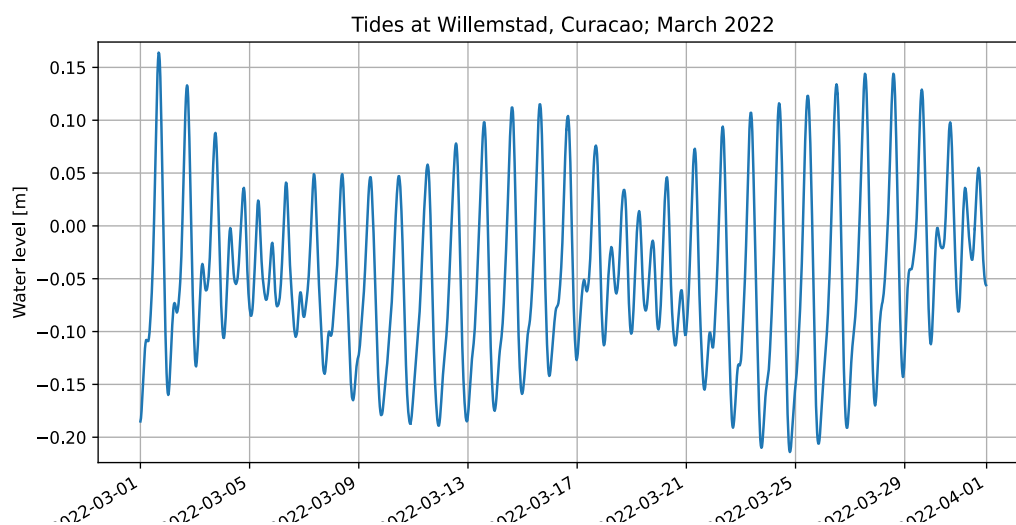


Figure 2: Variations in the water level (tide) around Curaçao for the month of March 2022

around coral reefs, and are a key factor in determining the success of reef-building species (Jackson-Bue et al., 2022). In shallow coastal waters, the presence of canopies, such as coral reefs, results in strong vertical wave and tidal current velocity gradients from the surface to the sea bottom, with velocity decreasing with depth (van Rooijen et al., 2020; Lowe et al., 2005; Hill, 1991). These vertical velocity gradients can enhance the mixing between nutrients and coral reef structures (van Rooijen et al., 2020). Using a computational model, Lowe et al. (2005) showed that oscillating flow that is generated by tidal currents resulted in a higher velocity around the canopy (coral reefs) when compared to unidirectional flow with the same velocity. Flow over coral reefs can change the diffusion of dissolved substances such as oxygen (Badgley et al., 2006; Stocking et al., 2018).

#### 1.4 Oxygen mechanisms of coral reefs

Coral reefs rely on environmental factors to ventilate their external surface as they lack a mechanism to do so themselves. Like all aerobic organisms, coral reefs consume oxygen during respiration, and the amount of oxygen available is dependent on several factors, both environmental and physical (Nelson & Altieri, 2019). Oxygen is exchanged between coral and the surrounding water by diffusion, a process that is triggered by an oxygen gradient, with oxygen moving from areas of high concentration to low concentration. Diffusion is also influenced by the local hydrodynamic conditions, with a higher rate of diffusion in high flow areas (Finelli et al., 2006). Symbiotic zooxanthellae, a photosynthetic alga, live on coral reefs and produce oxygen, and coral reefs almost immediately consume that oxygen (Kühl et al. 1995; Nelson & Altieri, 2019). The zooxanthellae use the products of coral respiration in photosynthesis, and coral use the products of photosynthesis in respiration (Gardella and Edmunds, 1999), creating a feedback loop between the respiration and production of oxygen. If the oxygen uptake rate of the coral is less than the production rate of the zooxanthellae, the coral has to release oxygen back into the water column in order to prevent a build-up of potentially toxic levels of oxygen. The rate of oxygen production from photosynthesis is faster than the uptake rate of coral reefs, leading to an expulsion of oxygen to the surrounding seawater by the coral (Mass et al. 2010). Slower flow results in less exchange of solutes between coral and the surrounding seawater, leading to an accumulation of oxygen, increasing oxidative stress.

Coral have the ability to stop respiration in low oxygen conditions in order to prevent depleting the available oxygen, although this is a very inefficient process for the animals (Gardella and

Edmunds, 1999). Oxygen is a keystone of reef health, and can be a limiting factor that determines growth and function.

## 2. Objectives and Problem Definition

Curaçao has year-round rainfall and lacks significant hills, leading to a large amount of land run-off, resulting in a high nutrient concentration in the surrounding waters. This possibly contributes to the decline of reefs around the island (Waitt Institute, 2017). An increase in nutrients and pollutants in water can cause turf algae to grow on coral rapidly, causing a decline in coral growth and health. Vermeij et al. (2010) found an increase in turf algae on Curaçao reefs, leading to concern for recent reef health. De Bakker et al. (2016) and Waitt (2017) found a decline in shallow fore-reef hard coral cover of 79% between the 1980s and 2015. The decline of coral cover around Curaçao is shown in figure 3.

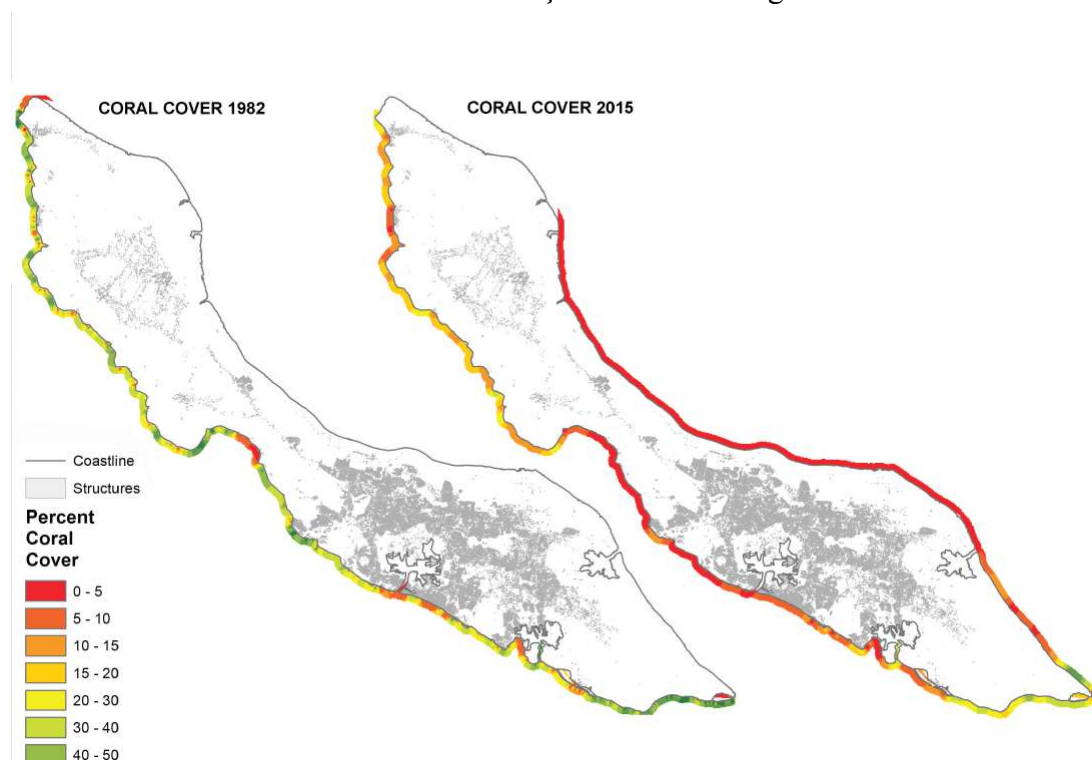


Figure 3: Coral cover in 1982 and 2015, taken from the Waitt Institute (2017). There is no north shore data for 1982

As hard coral reefs continues to decline, reef communities have been undergoing phase shifts towards algal cover, potentially limiting the ability of corals to regrow in these algal dominated areas (de Bakker et al., 2016). Healthy reef structures provide vital protection from coastline erosion and storm surges by increasing sea bottom roughness and friction, however, the steady take over by algae is decreasing this coastal protection (McCook et al. 2001).

As part of a larger project, SEALINK, that is investigating how land-derived inputs impact the survival and growth of coral reef in the Dutch Caribbean (NWO, 2021), this thesis project seeks to collect field data to investigate whether a relationship exists between hydrodynamics and dissolved oxygen near coral reefs around Curaçao. The data will be applied to computational fluid dynamics (CFD) models to improve the predictive results of future models. For the purpose of this project, data was gathered on waves, currents, and dissolved oxygen to determine their impact on coral reefs.

## 2.1 Research questions

The main research question investigated during this thesis is as follows: Are coastal hydrodynamics contributing to local dissolved oxygen fluctuations around coral reefs on Curaçao?

Three sub-questions were developed:

### 2.1.1 Sub question 1

Are waves and currents measurably different around the island? What are these differences and to what extent are they different?

### 2.1.2 Sub question 2

Can the found differences in waves and currents be used to predict the level of dissolved oxygen near coral reefs?

### 2.1.3 Sub question 3

What can numerical models teach us about the impact of water flow on dissolved oxygen fluctuation?

Chapter 1 of this report starts by introducing Curaçao and the study subject, followed by the research parameters and current knowledge on the subject. Chapter 2 details the objectives of this project, followed by research questions. Chapter 3 details the methodology, including instruments used, field work set up, data analysis, CFD model creation, and elaborates on the study locations. Chapter 4 presents the results of the field campaign and computational models, and chapter 5 interprets the results, reflecting on the combination of fieldwork and computational model use. The discussion at the end of chapter 5 seeks to answer the research questions formulated in chapter 2, and gives recommendations for future research.

### 3. Methods

During a month-long fieldwork campaign, conducted with myself and PhD candidate Vesna Bertonecelj, in-situ data was collected in order to investigate the relationship between flow and dissolved oxygen fluctuation near coral reefs around the island of Curaçao.

#### 3.1 Location

Seven study sites, shown in figure 4, on the south-facing coast of Curaçao were chosen based on water quality data results from November 2021, and their position around the island. The sites cover three main areas: the west point, east point, and middle of the island. These were chosen to get thorough insight into water flow and oxygen movement along the southern

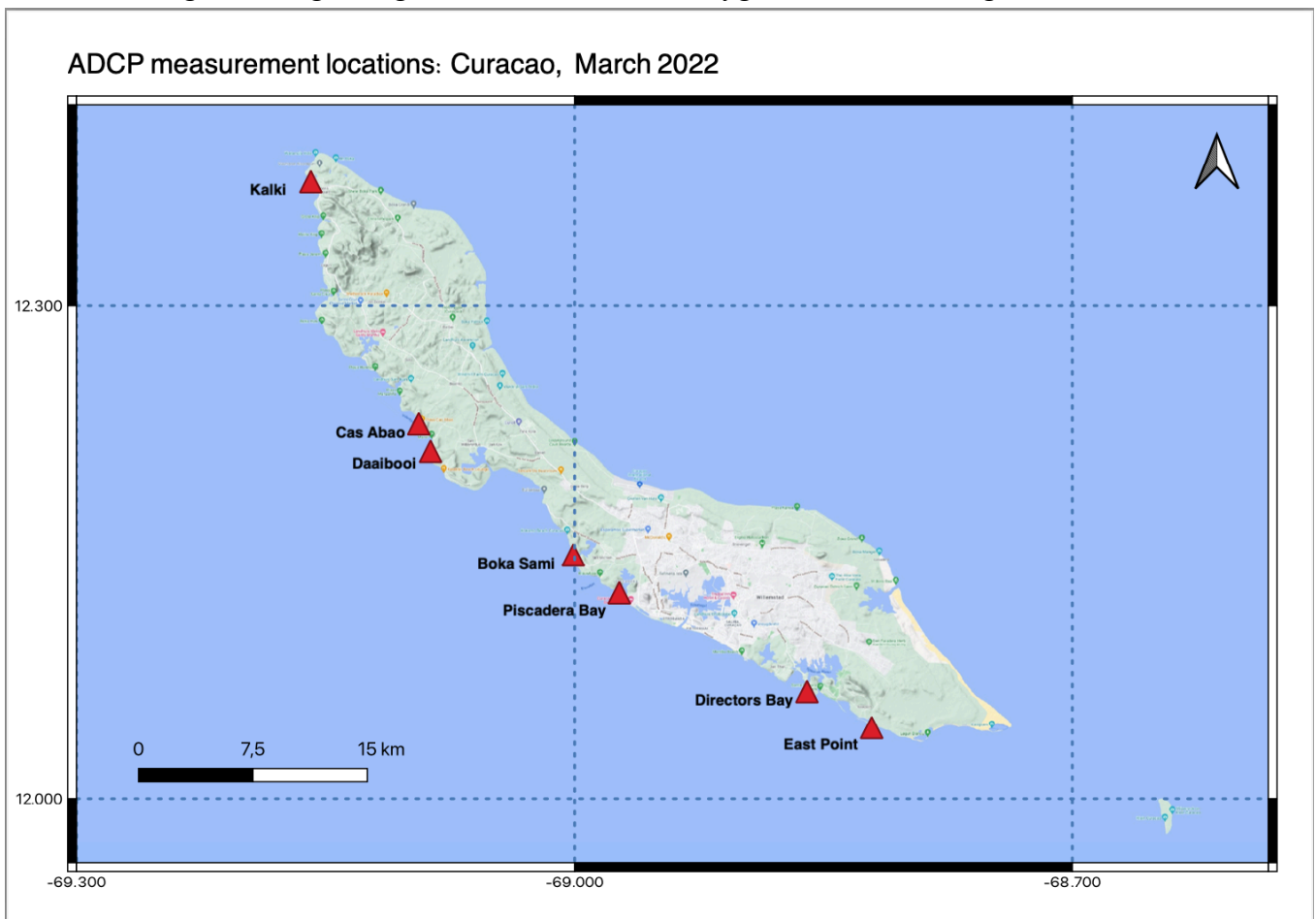


Figure 4: Sampling locations for AD2CPs and MiniDOTs. All location accessed via beach, except for East Point and Piscadera Bay (accessed via boat)

coast. Each study site was sampled at least two times, with the exception of East Point (due to difficulty of deployment); once during spring tide, and once during neap tide (fig 2).

Playa Kalki, nicknamed Alice in Wonderland for the diversity of colorful animals and coral reefs, is located near the north-western tip of the island and is characterized by sand flats and a

moderate coral slope (Padi Travel, 2021). Cas Abao beach, located south of Playa Kalki, is characterized by layers of coral slopes approximately every five meters. Daaibooi is located between two cliffs, with the reef starting at the end of the cliffs where they open into the bay. The reef is fairly sparse, with medium-sized coral dominating at 10 meters depth. Boka Sami (located in Sint Michiel) is characterized by fairly new reef on the reef-flat, as most of it was destroyed in 2019 in a shipping explosion. About 10 meters offshore, the reef slopes down at a 45-degree angle, and is mostly dominated by brain coral that survived the accident (Dive Curaçao, 2022).

Piscadera Bay, located near the Caribbean Research and Management of Biodiversity (CARMABI) research station, is characterized by large reef flats and a sharp drop-off. The study area was to the right of the bay, and is relatively untouched by tourists as there is no public access by shore (only by boat). Director's Bay is the furthest south-eastern public beach, with diving accessible by shore. The reef is characterized by an abundance of coral and marine life. The reef flat extends to the left of the beach, about 20 meters offshore, then moves into a steep drop off (Dive Curaçao, 2022). East Point is only accessible by boat, has extremely strong currents, and boasts almost pristine, huge reefs, consisting of both hard and soft coral (Dive Curaçao, 2022).

### 3.2 AD2CP setup

Acoustic Doppler current profilers (ADCPs), introduced in the 1980s, are used in a wide variety of oceanography studies. ADCPs utilize the Doppler effect to measure water velocity by transmitting sound beams or pulses and measuring the time it takes for the sound to return to the instrument. The sound is reflected by particles in the water, not the water itself. In this way, it uses the particles as tracers, assuming that the particles are passive and moving at the same speed as water. The change in sound frequency is used to calculate the velocity of the particles based on the change in their position relative to the stationary instrument (Nortek, 2022). The instruments have the capability to measure current velocities along different depth profiles (Guerra & Thomson, 2017). More advanced ADCPs, such as the Nortek Signature 1000 AD2CPs, have the ability to measure currents, waves, and turbulence simultaneously, leading to a richer data set from each deployment. For this reason, these AD2CPs were chosen for the study. Two Nortek Signature 1000 AD2CPs were used during each deployment to measure average current velocities, turbulence (measured as “Burst” on

the device), and waves at the study locations. The AD2CPs were placed on the seafloor at depths between 5 and 10 meters. Special aluminium frames were built to hold the AD2CPs about 16 centimeters off the seafloor, as seen in figure 5.



Figure 5: AD2CP setup in metal frame

### 3.3 MiniDOT setup

The dissolved oxygen (DO) concentration near brain coral reefs structures was measured using two PME miniDOT Dissolved Oxygen Loggers. The devices measure DO and temperature at a single location over time. Each oxygen sensor was set to measure DO concentration and temperature every 1 minute, over a total time period of 6 hours on average. The sensors were placed on the sea floor about 15 centimeters away from a single *D. strigosa*, shown in figure 6, in order to prevent the sensors from touching the coral. Each sensor was attached to a dive weight in order to keep it on the sea floor, and video footage was taken to mark the location.



Figure 6: PME miniDOT oxygen logger near *D. strigosa*.

### 3.4 Fieldwork

Two Signature 1000 AD2CPs from Nortek and two PME miniDOT Dissolved Oxygen Loggers were used. The AD2CPs and miniDOTs were deployed together in one dive from the beach, twice from a boat during a boat dive, and retrieved at least 6 hours later. Figure 7 shows the set up used to transport the AD2CPs and PME miniDOTs. Two dive balloons were used to assist in the underwater transport of all instruments to the study sites. Attached to each dive balloon was one AD2CP and one PME miniDOT. Once each site was reached, each AD2CP was placed on the sea floor in a relatively flat spot near coral, with a miniDOT sensor placed near each



Figure 7: Transportation of the AD2CP and PME miniDOT. The orange dive balloon was attached to the AD2CP frame and oxygen logger via removable clips

AD2CP as close to a *D. strigosa* structure as possible. The AD2CPs were placed at least 5 meters apart in order to avoid crossing Doppler beams and to limit noise in the data. The measurements started recording .75 m above the sea bottom, to take into account the height of the AD2CP (.5 m) and a blanking distance of .25 m above the instrument where particles were too close to the top of the instrument to get an accurate measurement. Each deployment, except for East Point, lasted roughly six hours (table 1), dependent on the weather, sea conditions, and deployment start time. At the end of deployment time, the instruments were retrieved again via diving and brought back on land. Dependent on reef structure and orientation, cross-shore (perpendicular to the shore) and along-shore (parallel with the shore) configurations were chosen for each site in order to analyze the wave transformation and variability around corals in similar environments. A cross-shore configuration can potentially show wave transformation and dissipation across a reef flat, while along-shore configurations can help in the assessment of variations in currents and waves not due to a change in depth (e.g. different reef features and structures).

Table 1 details the deployment plans for each of the study sites and dates. The start and end time pertain to data collection while the instruments were in the water. Depth1 refers to AD2CP1 and depth 2 is ADCP2. The depth refers to the depth over which data was collected, but this does not necessarily reflect the depth at which the AD2CP was placed (from the seafloor to surface). All data was checked for corrupt and missing data, the start and end times were adjusted based on when the instruments were set up at or collected from the study sites. The data at the surface of the water was thrown out due to reflection with the sea surface. Descriptions of each plan can be found in appendix A.

<i>Date</i>	<i>Location</i>	<i>Latitude</i>	<i>Longitude</i>	<i>Start Time (UTC)</i>	<i>End Time (UTC)</i>	<i>Depth1 (m)</i>	<i>Depth2 (m)</i>	<i>Orientation</i>	<i>Plan</i>
8-3-22	Boca Sami	12.148003	-69.000541	14:45	21:05	8	4	Cross-shore	A
11-3-22	Kalki	12.375244	-69.159018	15:30	20:20	7	2	Cross-shore	A
13-3-22	Directors Bay	12.065077	-68.859796	14:15	18:11	3	12	Cross-shore	A
15-3-22	Daaibooi	12.211274	-69.086790	13:50	19:41	8	3	Cross-shore	B
17-3-22	Piscadera Bay	12.124883	-68.973347	13:40	19:42	8	3	Cross-shore	C
18-3-22	East Point	12.043060	-68.821126	14:00	18:39	9	8	Along-shore	D, E
20-3-22	Boca Sami	12.148003	-69.000541	14:19	19:42	8	3.25	Cross-shore	F, G
21-3-22	Kalki	12.375440	-69.158875	14:00	20:02	7	7	Along-shore	F, G
23-3-22	Daaibooi	12.211274	-69.086790	14:10	20:12	9	9	Along-shore	F
25-3-22	Piscadera Bay	12.125097	68.973128	14:00	19:42	7	7	Along-shore	I, H
28-3-22	Directors Bay	12.065077	-68.859796	14:10	20:12	6	3	Cross-shore	J, K
29-3-22	Cas Abao	12.227895	-69.093898	14:00	20:12	8	8	Along-shore	I, H
30-3-22	Boca Sami	12.148003	-69.000541	13:55	20:07	9	8	Along-shore	F, H
1-4-22	Cas Abao	12.227801	-69.093696	14:00	19:32	8	7	Along-shore	H, I

Table 1: Metadata for the AD2CP deployments.

### 3.5 Modelling

To simulate water flow and dissolved oxygen movement near coral, a 2D numerical model was developed in the COMSOL mathematical modelling software. A rectangular box of 10 m by 2.5 m was created containing one .5 m tall half-sphere, with a radius of 180 degrees, to simulate a brain coral. The coral was placed at 6 m in order to allow flow to develop before interacting with the coral. Water and oxygen were forced through the inlet boundary (1 in fig 8), the water and oxygen outlet boundary is marked by 5 in the figure, 6 is an open boundary to simulate the in-situ study area that was

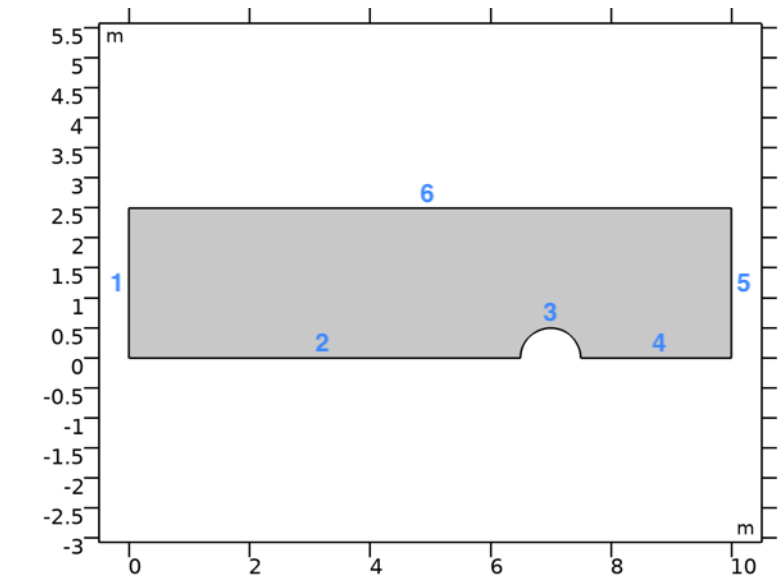


Figure 8: Modelled geometry, with one coral reef. 1 marks the inlet, 5 is the outlet, 2-4 are walls, and 6 is an open boundary. The y-axis shows the height of the box in meters, and the x-axis shows the width of the box in meters.

open to the ocean, and 2-4 were treated as solid boundaries (called walls in the model). Two physics properties were modelled: laminar water flow and the transport of a diluted species (oxygen in this case). All parameters of the model can be found in Appendix B.

The diffusion and advection of water and oxygen particles through the modelled environment were tested using velocity values from field data at Boca Sami on March 8<sup>th</sup>, 2022.

Fluid flow was calculated using the following Navier-Stokes equations for time-dependent, incompressible laminar flow:

$$\rho \nabla \cdot \mathbf{u} = 0 \quad (1)$$

$$\rho \frac{\partial \mathbf{u}}{\partial t} + \rho (\mathbf{u} \cdot \nabla) \mathbf{u} = \nabla \cdot [-p\mathbf{I} + \mathbf{K}] + \mathbf{F} \quad (2)$$

The above equations are two of the Navier-Stokes equations, with equation 1 representing the conservation of mass, and equation 2 representing the conservation of momentum.

$\rho$  is the density of water ( $\text{kg/m}^3$ ),  $\mathbf{u}$  is the velocity vector ( $\text{m/s}$ ),  $p$  is the pressure (Pa),  $t$  is time (s),  $\mathbf{I}$  is the identity matrix,  $\mathbf{K}$  is the viscous stress tensor (Pa), and  $\mathbf{F}$  is the volume force

vector (N/m<sup>3</sup>). Additional equations were applied to calculate the transport of a diluted species:

$$\frac{\partial c_i}{\partial t} + \nabla * \mathbf{J}_i + \mathbf{u} * \nabla c_i = R_i \quad (3)$$

$$\mathbf{J}_i = -D \nabla c \quad (4)$$

$$\frac{\partial c}{\partial t} = \nabla * \mathbf{J}_i + R \quad (5)$$

Where  $c_i$  denotes species concentration (mol/m<sup>3</sup>),  $\mathbf{J}_i$  is the diffusive mass flux vector (mol/(m<sup>2</sup>\*s)), and  $R_i$  is the reaction rate for the chemical species (mol/(m<sup>3</sup>\*s)). Equation 4 is used in boundary condition and flux computations, and therefore includes the parameter,  $D$ , which is the diffusive coefficient (m<sup>2</sup>/s). A no slip condition, where  $\mathbf{u} = 0$ , was applied to the walls in figure 8 (numbers 2-4 in figure 7).

The Reynolds number, which determines how rough water flow is, was calculated by equation 6:

$$\frac{\rho * u * L}{\mu} \quad (6)$$

Where  $L$  is the length (m) of the environment, and  $\mu$  is the dynamic viscosity of water (Ns/m<sup>2</sup>). 10-minute averaged velocity values .75 m above the seafloor were used as the input velocity in an interpolation

function over time, shown in figure 9. The values can be found in table 2 located in Appendix B1. The velocity values changed every 30 seconds over the entire length of the simulation in order to mimic the rate of change seen in the velocity data on a smaller time scale. One modelled environment with one coral was created, and five simulations were tested: two with a fixed water

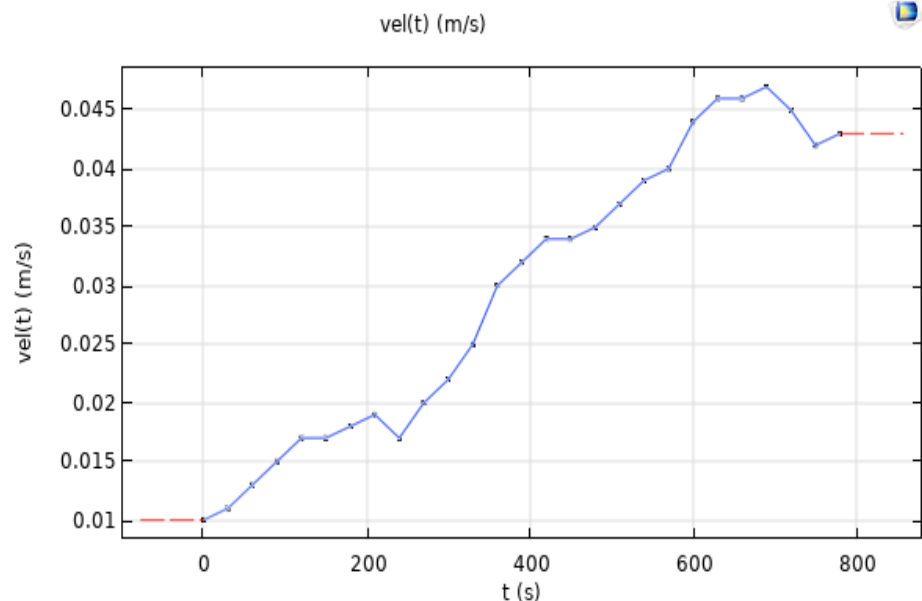


Figure 9: Interpolated velocity values over time. Velocity (m/s) is shown on the y axis, and time (s) is shown on the x axis.

viscosity value and a change in diffusion rates, and two with a fixed diffusion rate and changed viscosity values. A fifth simulation was run with a constant velocity of .01 m/s that switched direction halfway through the simulation, and fixed diffusion and viscosity values. These five simulations were tested in a time-dependent study and a stationary (i.e. not time-dependent) study. The first four time-dependent studies were limited to 800 seconds (13 minutes and 20 seconds) based on the ability of the simulation to run successfully, and had a time-step of .1 seconds, while the fifth simulation was able to run for 3000 seconds (50 minutes) given available computational resources. For the stationary study, the time-differential term in equation 2 was ignored in order to visualize the effects of diffusion and viscosity without the time limitation.

### 3.5.1 Granger Causality

Many statistical tests can be used to show the connectivity between time series data sets, however, only a few demonstrate causality between elements. The Granger causality time series test analyzes time series with common trends to see if the past values (defined as time-lagged or delayed values in this test) of a series can be used as a predictor of another (Tirabassi et al., 2015). Granger (1969) defined causality as

*If some series,  $Y_1$ , contains in past terms that helps in the prediction of  $X_1$ , and if this information in no other series used in the predictor, then  $Y_1$  is said to cause  $X_1$ .*

Understanding this predictive definition and knowing how to apply it can help improve predictive models for climate and environmental data, although it has been used in few studies to date. The Granger causality tests a null hypothesis against an alternative hypothesis, and compares the remainders of the alternative hypothesis with the null. (Mosedale et al., 2006; Barnett & Seth, 2014; Calhoun et al., 2017). If the prediction of one value can be improved by using the other value as a predictor, the predictor value is then said to be causal for the first value.

The Granger causality approach was used in this thesis to quantitatively assess the effect of current velocities on dissolved oxygen concentration in the chosen study sites around Curaçao. A Python script taken from Susan Li (Li, 2020) and adapted by Paolo Stocchi, was used to assess the Granger causality. In order to use this causal test, the data sets must be statistically stationary, i.e. the distribution does not change temporally. The data sets used here first needed to be adjusted to remove the time-dependence and become stationary. The

developed null hypothesis (i.e. with no possible causality) was then tested against the alternative hypothesis.

The null hypothesis for the data sets used in this thesis was determined to be, “North and east water velocities are not useful for predicting dissolved oxygen values,” and the alternative hypothesis was determined to be, “North and east velocities are useful for predicting dissolved oxygen values.” The probability of obtaining observed results (assuming that the null hypothesis is correct) is known as the p-value. If the p-value is below a specified threshold, the null hypothesis can be rejected, and the alternative hypothesis accepted. The significance level of the p-value was chosen as .05, meaning that if the p-value is found to be below this number, then the null hypothesis can be rejected. The velocity and DO data used for the test was 10-minute time averaged because this was the shortest time-step available for velocity.

## 3.6 Data Analysis

For the data analysis, Python was used for plot visualizations, and the AD2CP data was processed using the Ocean Contours software from Ocean Illumination, which has specialised algorithms to calculate wave data and visualise average current data. An extensive Python script was created by PhD candidate Vesna Bertoneclj to visualize the current velocities, wave height, pressure, and DO in the same time frame.

### 3.6.1 Current velocities

The current data from each AD2CP was loaded into the Ocean Contours processing software and the data was adjusted to exclude data recorded when the instruments were out of the water. Data from the surface of the water and above was also discarded. A threshold for side-lobe interference, the spill-over of energy as the sound waves from each beam interact with boundaries on the way up to the top of the measuring range, was set to 90%. This is the recommended value from the instrument manual as it results in the least amount of noise in the data set. The minimum correlation threshold was set to 50%, and any data below that was deemed to be no good and discarded. The resulting data set was then averaged over every 1 meter for 30 minutes, and an output file compatible with Python was created.

### 3.6.2 Wave data

The wave data was processed in a similar manner as the current data. Ocean Contour has a specific wave processing module that automatically creates a threshold for good data and masks anything below that threshold. The data from both AD2CPs was processed using a method called the Maximum Likelihood Method, which is a method of estimating parameters of an assumed probability distribution given some observed data. AD2CP2 used this with surface tracking, and AD2CP1 did not use surface tracking due to the deployment plans being incompatible with this feature.

### 3.6.3 Dissolved oxygen data

Dissolved oxygen data from the PME miniDOTs was downloaded from each logger as a comma separated values (csv) file, then first visualised in Excel to get a general idea of the DO and temperature trends of each site. The data for each logger was analysed further using a Python script that plotted the DO and temperature time series against one another in the same plot. This helped to quickly visualize potential trends in the data.

## 4. Results

This chapter details the results of the fieldwork campaign and the numerical model, which will be further interpreted in the discussion. First, the field data for hydrodynamics and dissolved oxygen for all sites are presented as well as the results of the statistical analysis tests run on the data (4.1). All time stamps were recorded in Coordinated Universal Time (UTC).

### 4.1 Results of fieldwork

#### 4.1.1 Along-shore

The AD2CPs were placed at two ends of a line transect parallel to the shore. For study sites where both data collection days were along-shore, or parallel with the shoreline, current velocities, east (V) and north (U) showed similar processes.

### **Daaibooi March 23, 2022**

Figure 10 shows current velocities from Daaibooi beach on March 23, 2022. The AD2CPs were set up according to plan F (table 1, Appendix A) in an along-shore configuration at 9 meters depth. At the site of AD2CP1, a southward flow was dominant in the first 1.5 hours (fig 10 c), with very little velocity in the east or west direction (fig 10 d), varying between east and west, from  $-0.012$  to  $0.012$  m/s. A large part of the day in this location (15:30 to 19:45 UTC) was dominated by a stronger northward flow, ranging from  $0.01$  to  $0.06$  m/s. There was a peak in northwest flowing current around 18:00, right before the tide reached low time (fig 10 e and j). The velocities showed a lot of variation over the depth of the measurements (from seafloor to surface), with the strongest currents in the upper 2 meters of the water column. AD2CP2 showed a similar increase in northwards velocity, from 15:30 to 19:30 UTC, and showed stronger velocities in the east and west direction (fig 10 h-i). The data from this day showed complex current velocities with lots of change over time and depth. For both AD2CPs, maximum wave height peaked around the same times of day, possibly following the tidal cycle (fig 10 b, e, g, j), although the significant and maximum wave heights were higher at the site of AD2CP2. Both AD2CPs show a peak wave height around 17:15 UTC, with AD2CP1 data at  $.5$  m and AD2CP2 data at  $.65$  m. AD2CP1 shows a relative increase in wave height when velocities are flowing north, although the peak happened when an eastward velocity was dominant, with an almost  $0$  m/s velocity in the north or south direction higher in the water column. The AD2CP1 wave height measurements appeared to plateau in the  $.3$ - $.35$  m range after the peak height at 17:15 UTC. The wave heights for AD2CP2 also decreased after the peak height, but increased again in the last hour of measurements. Dissolved oxygen at both AD2CP locations followed similar trends. Each miniDOT logger was placed close to its corresponding AD2CP as close to a brain coral as possible. There was an hour-long time window at the beginning of the collection period (fig 10 a and f), from 14:45-15:45, where DO increased initially, then decreased as velocities got stronger. There were two more clusters of notable DO increase around 18:00 and again from 19:45 to the end of collection. In both miniDOT loggers, there was a sharp decrease in DO concentration right before the last peak, around 19:30.

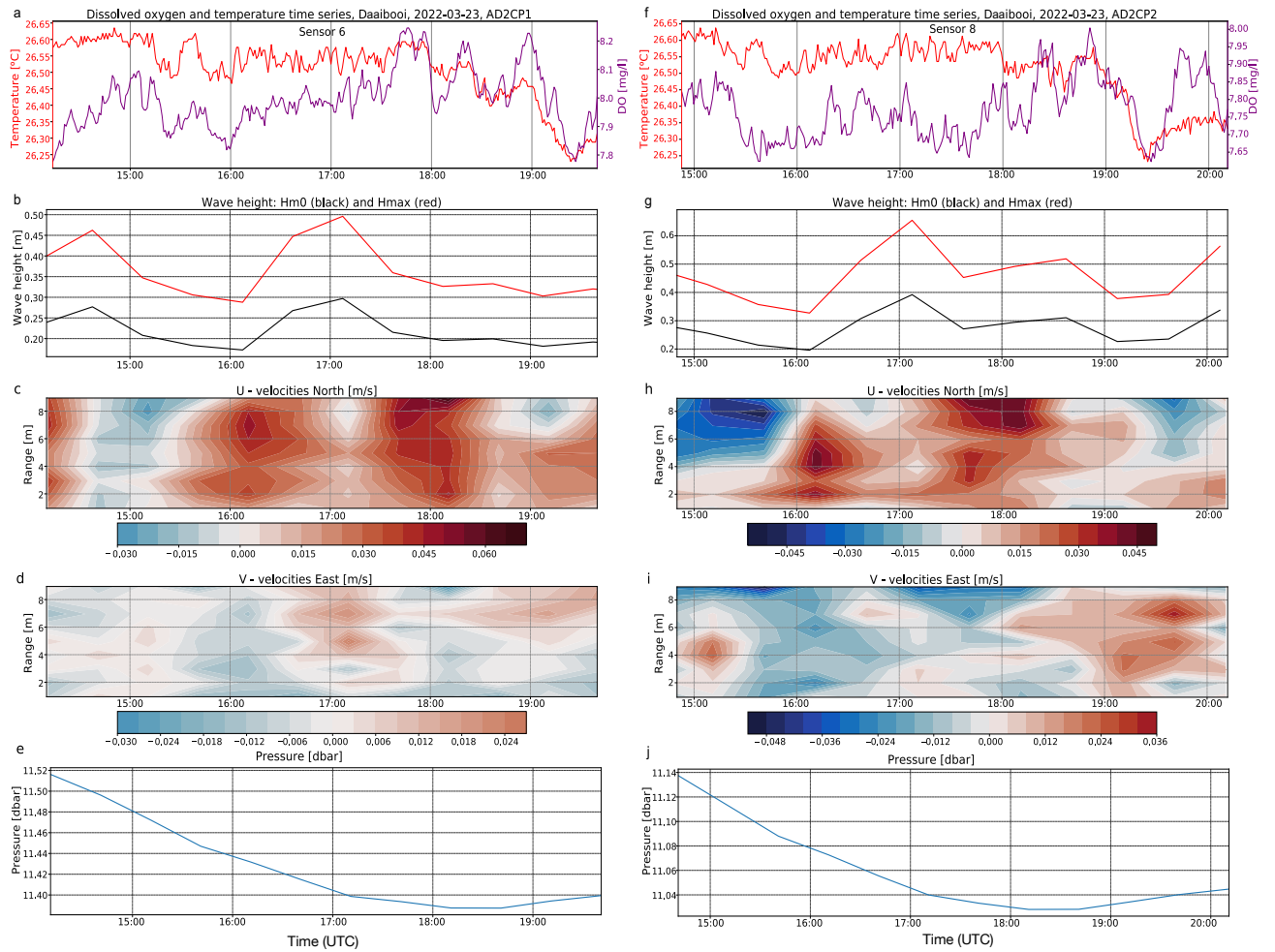


Figure 10: Field data from Daaibooi beach on March 23, 2022. From top to bottom: Dissolved oxygen (mg/L) and temperature (C), wave height – significant ( $H_{m0}$ ) and max ( $H_{max}$ ) (m), north velocity (m/s), east velocity (m/s), and water pressure (dbar). The range (m) is the depth from the AD2CP to the surface. The left graphs are from AD2CP1 and the right are from AD2CP2. Blue indicates a negative velocity and the opposite direction of the labeled graph, i.e. south or west direction. Range on the y axis for the velocity graphs refers to the depth of measurement

### Kalki March 21, 2022

The AD2CPs at Kalki on March 21, 2022 were set up according to plan F for AD2CP1 and G for AD2CP2 (Appendix A). The data from AD2CP2 was unusable due to an error in the instrument data collection. Figure 11 shows the hydrodynamic data and DO data for this site. The current velocity data from AD2CP1 showed very strong velocities in the northward direction for the entire measurement time, however there was a southward flowing weak bottom current in the bottom 1 meter (fig 11 c). There were two periods of stronger northward current, one from 15:00-16:00 and the other from 19:00 to the end of the measurement period. These increases in northward velocity coincided with increases in the westward current and occurred just before and after low tide (fig 11 e).

The maximum wave height had an average of .5 m, with a final peak of .58 m coinciding with the peak in northward velocity, at .15 m/s (fig 11 b-c). There was a slight increase in wave

height during the bottom current increase from 17:00-18:00 (fig 11 c and d). There were two peaks in wave height that coincided with the increase in velocities just before and after low tide. Higher pressure corresponds to high tide, and lower pressure corresponds to low tide.

Figure 11 a, displaying DO concentration, showed a decrease in DO in the last hour of the measurement time, that coincided with the last peak in current velocity, pointing to a potential connection between the two. There was a peak in DO around 16:30, during a decrease in velocity and wave height. There was a steady increase in concentration for the first 2.5 hours. DO decreased towards the end of the time series, coinciding with the peak in current velocity.

### Cas Abao March 29, 2022

Figure 12 shows the hydrodynamics, water pressure, and DO from Cas Abao on March 29<sup>th</sup>, and followed plans I and H for the AD2CPs (appendix A). There was a sudden switch from a southeast flow to a northwest flow around 15:30, with a velocity of 0.0 m/s around 15:50. This zone of no velocity occurred during a tidal switch from high to low tide (fig 12 e and j), with faster velocities at the surface and bottom. There was a slight delay in this switch seen in the east/west velocity plots, potentially due to inertia. The current velocity data from both AD2CPs showed a peak in north velocity starting around 15:50. This peak occurred from 6 m above the AD2CP to the surface. This peak lasted much longer in the AD2CP2 data, until 18:15, and showed a stronger velocity gradient down to the bottom. Both AD2CPs captured the tidal currents with no other oceanic processes visible.

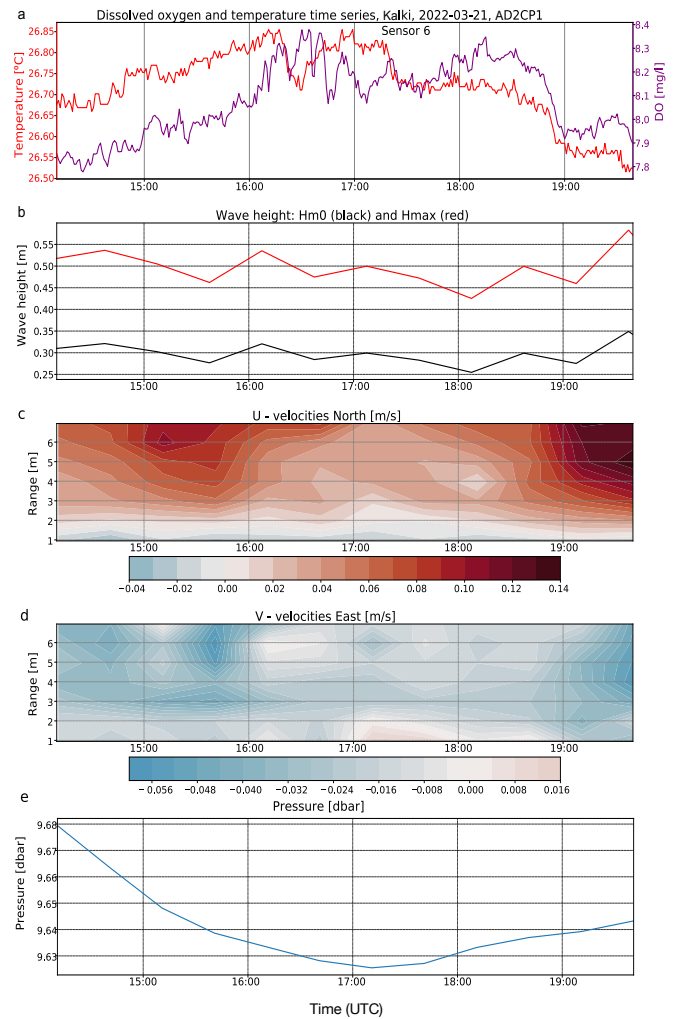


Figure 11: Field data for AD2CP 1 at Kalki beach on March 21, 2022. From top to bottom: Dissolved oxygen (mg/L) and temperature (°C), wave height (m), north velocity (m/s), east velocity (m/s), and water pressure (dbar). Blue indicates a negative velocity indicates the opposite direction of the labeled graph, i.e. south or west direction. Range on the y axis for the velocity graphs refers to the depth of measurement

AD2CP1 showed a peak wave height of .82 m around 15:45, whereas the peak wave height at AD2CP2 occurred much later, around 19:15 (fig 12 g). This peak occurred during the period of 0.0 m/s current velocity (fig 12). The increases and decreases in wave height from both AD2CPs followed the same pattern, but were more pronounced in AD2CP2. The lowest wave height occurred around 18:15, .42 m/s for AD2CP1 and .49 m/s for AD2CP2, coinciding with the peak current velocities.

The DO concentration near AD2CP1 had an increasing trend until 19:00 and then decreased for an hour before increasing again at the end of the measurement time. The data from both oxygen loggers were very different in trend, with sensor 8 (fig 12 f) showing larger variation in concentration. Both sensors varied between 7.8 and 8.5 mg/L, but sensor 8 reached peak value (8.3 mg/L) almost exactly two hours earlier. Sensor 6 (fig 12 a) gradually increased over time while sensor 8 (fig 12 f), fluctuated a lot over time.

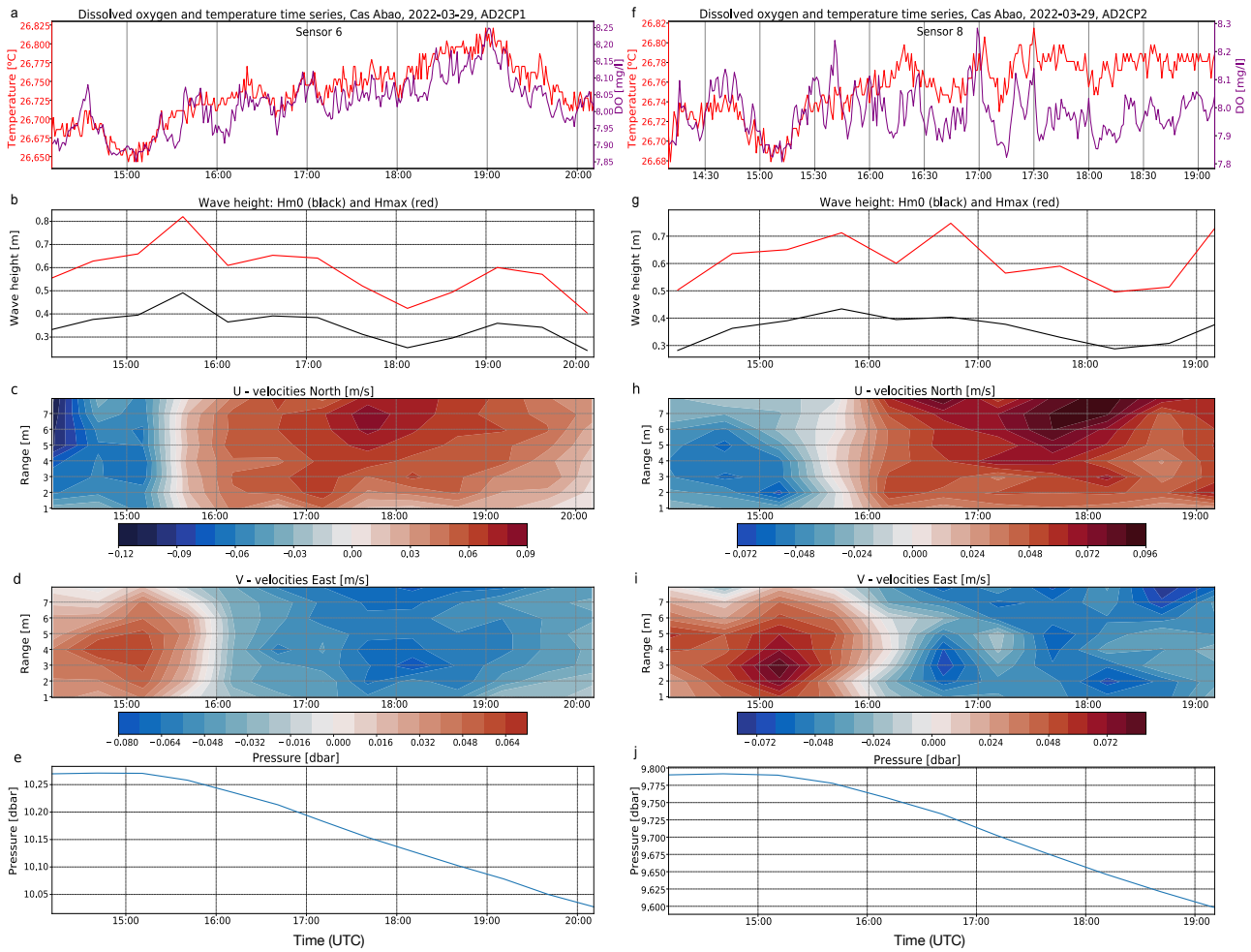


Figure 12: Field data from Cas Abao on March 29, 2022. AD2CP1 is on the left, AD2CP2 is on the right. From top to bottom: Dissolved oxygen (mg/L) and temperature (C), wave height (m), north velocity (m/s., east velocity (m/s), and water pressure (dbar). The right graphs are from AD2CP1 and the left are from AD2CP2. Blue indicates a negative velocity indicates the opposite direction of the labeled graph, i.e. south or west direction. Range on the y axis for the velocity graphs refers to the depth of measurement

### Cas Abao April 1, 2022

AD2CP1 and AD2CP1 were set up according to plans H and I respectively (Appendix A). The current velocities from Cas Abao on April 1<sup>st</sup>, shown in figure 13, were similar to the previous results from March 29<sup>th</sup> (fig 12), except the peak north velocity happened earlier in the day, around 16:50. The tide changed from low to high back to low tide, with the switch from high to low tide occurring much later in the day, just after 17:00 (fig 13 e and j). Unlike the previous results, there wasn't a southeast flow until the end of the measurement time, and only for about 1 hour, before the flow switched direction back to northwest. The north velocity from AD2CP1 was much stronger than AD2CP1 at the peak, .096 m/s compared to .075 m/ s. In AD2CP1, there were two periods of close to 0.0 m/s velocity in the east or west direction,

occurring between 2 and 7 m at 14:30 and 4 and 7 m at 17:50. These same instances can be seen in the AD2CP2 data as well, but the second period occurred between 1 and 3 m around 18:00 (fig 13 h).

The wave height for AD2CP1 followed a fairly consistent pattern of increasing and decreasing every hour, for the first half of the measurement period (fig 13 g). From 17:00 to 19:00, the wave height slowly decreased until it reached a low of .20 m, then increased for the rest of the data collection period. This increase can be seen in both AD2CP datasets, and coincided with the last directional switch of current velocities, as described above. This increase also corresponded to a switch from high to low pressure (fig 13 e and j), as the tide started to switch from high to low.

Both oxygen sensors followed the same pattern, with a low seen around 15:45, and a peak seen around 19:15 (fig 13 a and f). This last peak occurred at the same time as the directional switch in current velocity as described above, with a period of low flow as it switched. This low flow could explain why the DO spikes, because it followed patterns that have been seen at other sites, with high DO at low flow. Sensor 6 (fig 13 a) appeared to show slightly higher DO concentrations throughout the time series.

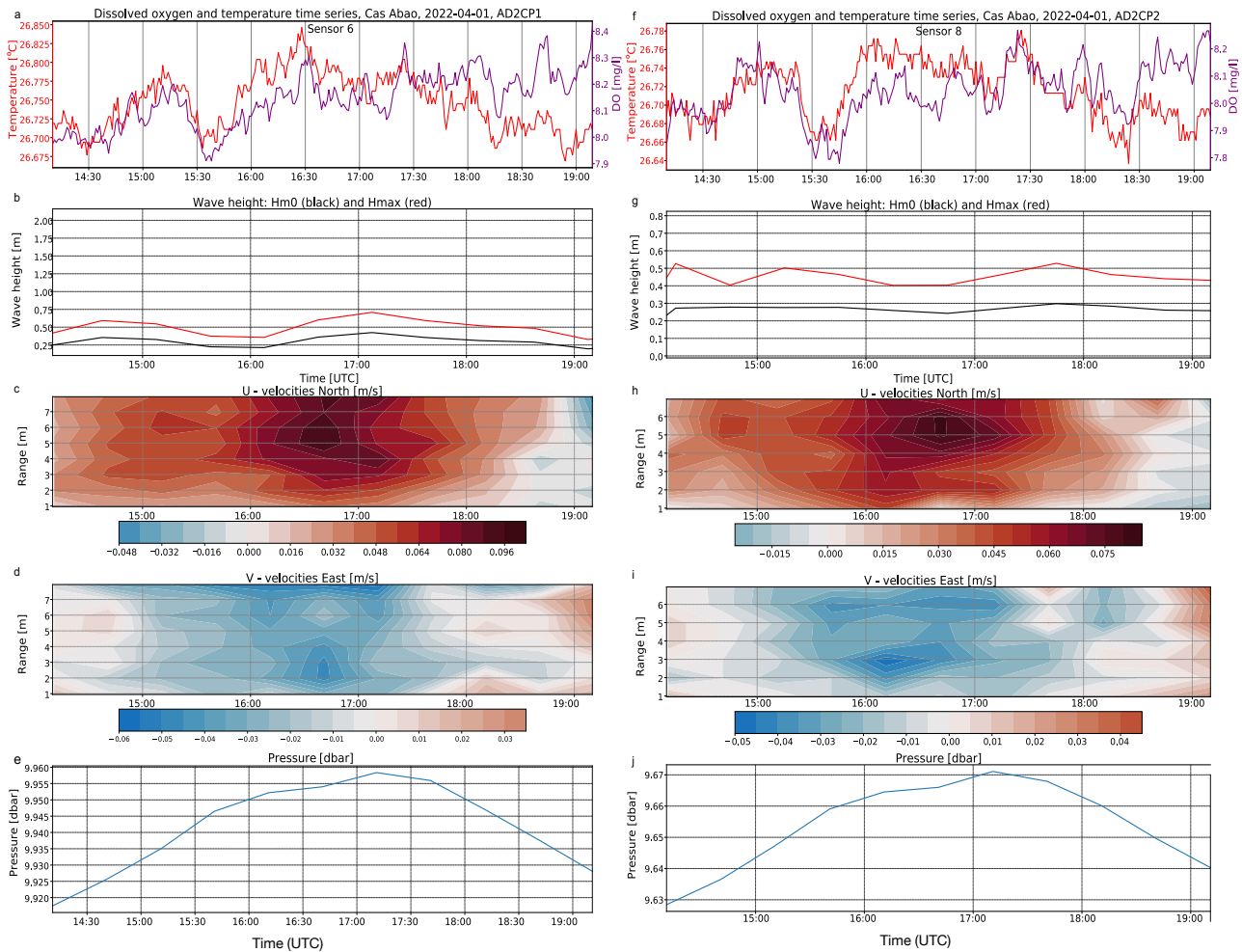


Figure 13: Field data from Cas Abao on April 1, 2022. AD2CP1 is on the left, AD2CP2 is on the right. From top to bottom: Dissolved oxygen (mg/L) and temperature (C), wave height (m), north velocity (m/s., east velocity (m/s), and water pressure (dbar)

### East Point March 18, 2022

Figure 14 shows data from East Point on March 18, 2022. AD2CP1 and AD2CP2 were set up according to plans D and E (Appendix A) East point was only accessible by boat, and typically has stronger currents and higher waves. This was very evident in the AD2CP data, showing an extremely strong current velocity for the entire measurement time (fig 14 c-d, h-i). AD2CP1 showed a peak velocity of .25 m/s in the west direction and .27 m/s in the north direction. The current was flowing in a northwest direction the entire measurement period, with the strongest currents in the top 3 meters of the surface. The last peak wave height, around 16:30, corresponded to the transition from high to low tide (fig 14 b, e, g, j). Both oxygen sensors showed a trend of increasing DO concentration, which corresponded to the decrease in velocity over time.

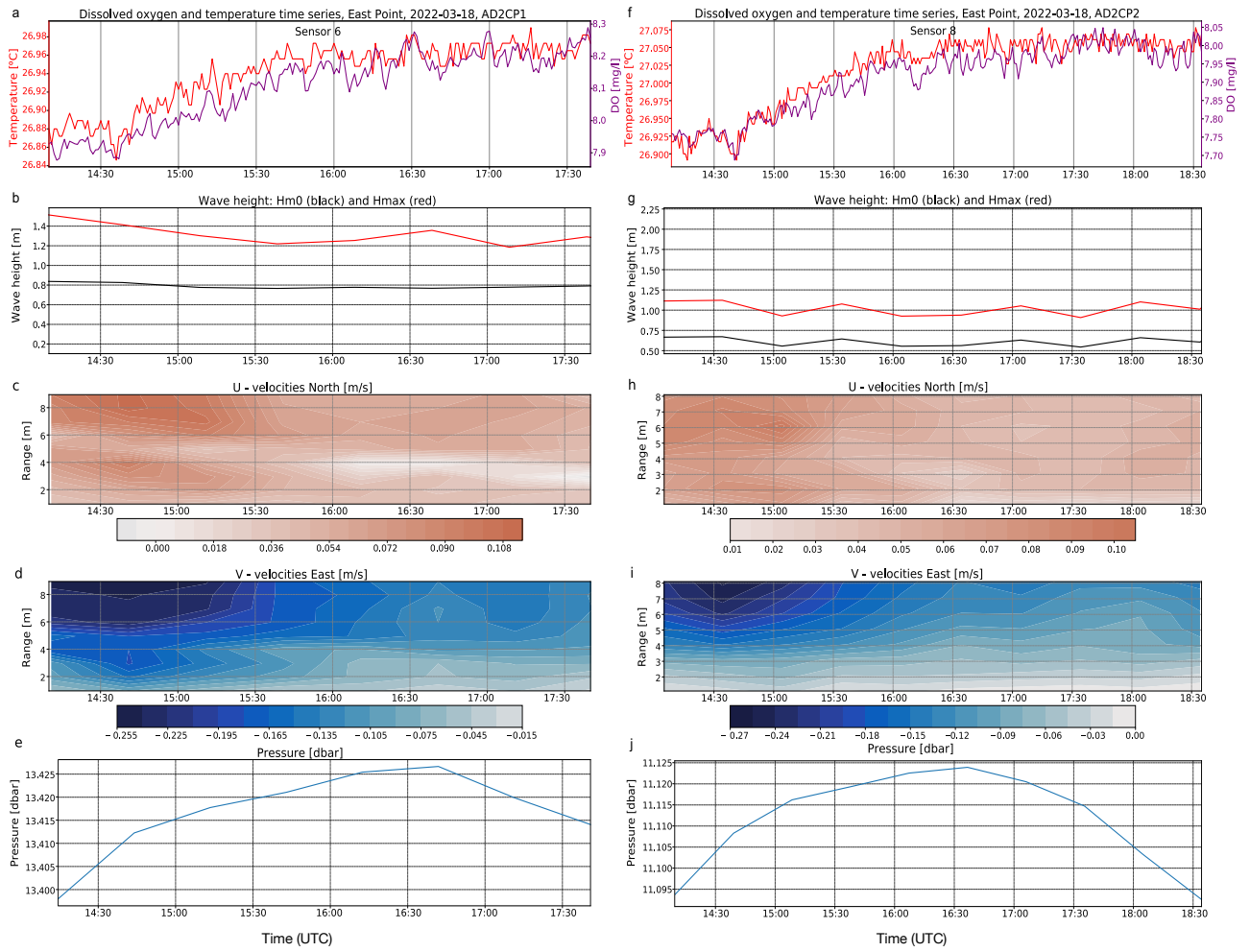


Figure 14: Field data from East Point on March 18, 2022. AD2CP1 is on the left, AD2CP2 is on the right. From top to bottom: Dissolved oxygen (mg/L) and temperature (C), wave height (m), north velocity (m/s), east velocity (m/s), and water pressure (dbar)

#### 4.1.2 Cross-shore

For study sites with the AD2CPs in a cross-shore, or perpendicular to the shore, configuration, east and north current velocities and dissolved oxygen concentrations were very different. Deployment details can be found in table 1.

##### **Boca Sami March 8, 2022**

Current velocities for both AD2CPs in a cross-shore configuration at Boca Sami on March 8, 2022, shown in figure 15, showed variations, with slightly higher velocities shown on AD2CP2, which was closer to the shore and at a shallower depth of 4 m. AD2CP1 (at 7 m depth) showed a weak northeast velocity for the first half of the data collection, throughout most of the sampling depth (fig 15 b and c). At 1 meter above the sea floor, there was a distinctive westward flowing bottom current for the entire duration of sampling (7.5 hours), with the north component still present. This bottom current was not present closer to shore, as seen in the AD2CP2 data (fig 15 g). AD2CP2 data showed an initial flow direction of southeast at very slow velocities (.016 m/s maximum). Both AD2CPs showed an increase in velocity strength overtime, with a maximum northwards velocity of 0.128 m/s around 20:00 at the top 3 meters of the sampling depth, that lasts until the end of the data collection. Both AD2CPs were set up according to plan A (table 1, appendix A). No wave data was collected at this location for this sampling day.

The dissolved oxygen concentration varied considerably throughout the collection time, from 9.3 mg/L at the highest to 7.8 mg/L at the lowest (fig 15 a and e). The peaks and valleys at both miniDOT locations followed similar patterns, with sensor 6 (fig 15 a) showing larger variability in the first half of sampling. There were three points of sudden decreases in DO concentration between 17:00 and 18:00, with a final decrease to the lowest concentrations for both loggers between 19:30 and end of collection for the miniDOT near AD2CP1, and between 19:45 and 20:45 for the miniDOT (sensor 8) near AD2CP2 (fig 15 e). The DO concentrations and current velocities appeared to coincide (especially between 16:00 and 21:00), with higher DO corresponding to a lower velocity and vice versa, however, this could be due the presence of the bottom current as described previously. The final DO decrease happened during the period of maximum velocity, possibly showing that higher currents in this location caused the drop in DO concentration.

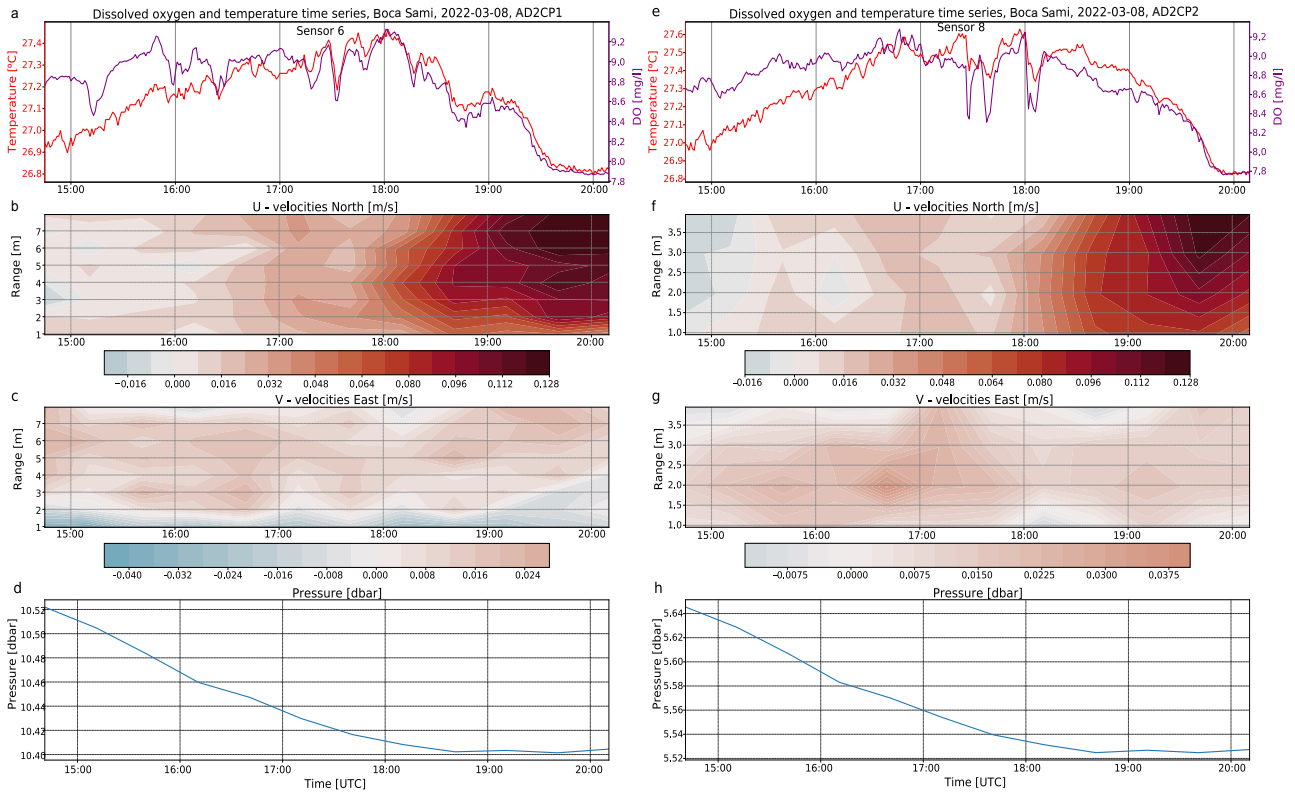


Figure 15: AD2CP and miniDOT logger data from March 8, 2022 at Boca Sami. From top to bottom: Dissolved oxygen (mg/L) and temperature (C), north velocity (m/s., and east velocity (m/s). The left graphs are from AD2CP1 and the right are from AD2CP2. Blue indicates a negative velocity indicates the opposite direction of the labeled graph, i.e. south or west direction.

### Kalki beach March 11, 2022

AD2CP1 shows a bottom eastward flowing current during the entire measurement period, shown in figure 16. From 17:30 to 19:00, there was a southward flow from 2 meters to the surface that switched between southwest and southeast halfway through this time period (fig 16 f-g). The pressure showed a slow switch from high to low tide, with a stronger northwest current towards the end of the time series (fig 16 h). AD2CP2 showed a very similar pattern with overall slower north/south velocities (fig 16 e-h).

Both oxygen sensors showed the same pattern of decreasing during the first hour of measurements, then increasing as velocity slows down (fig 16 a and e). There was a peak in concentration during the last velocity increase around 19:20.

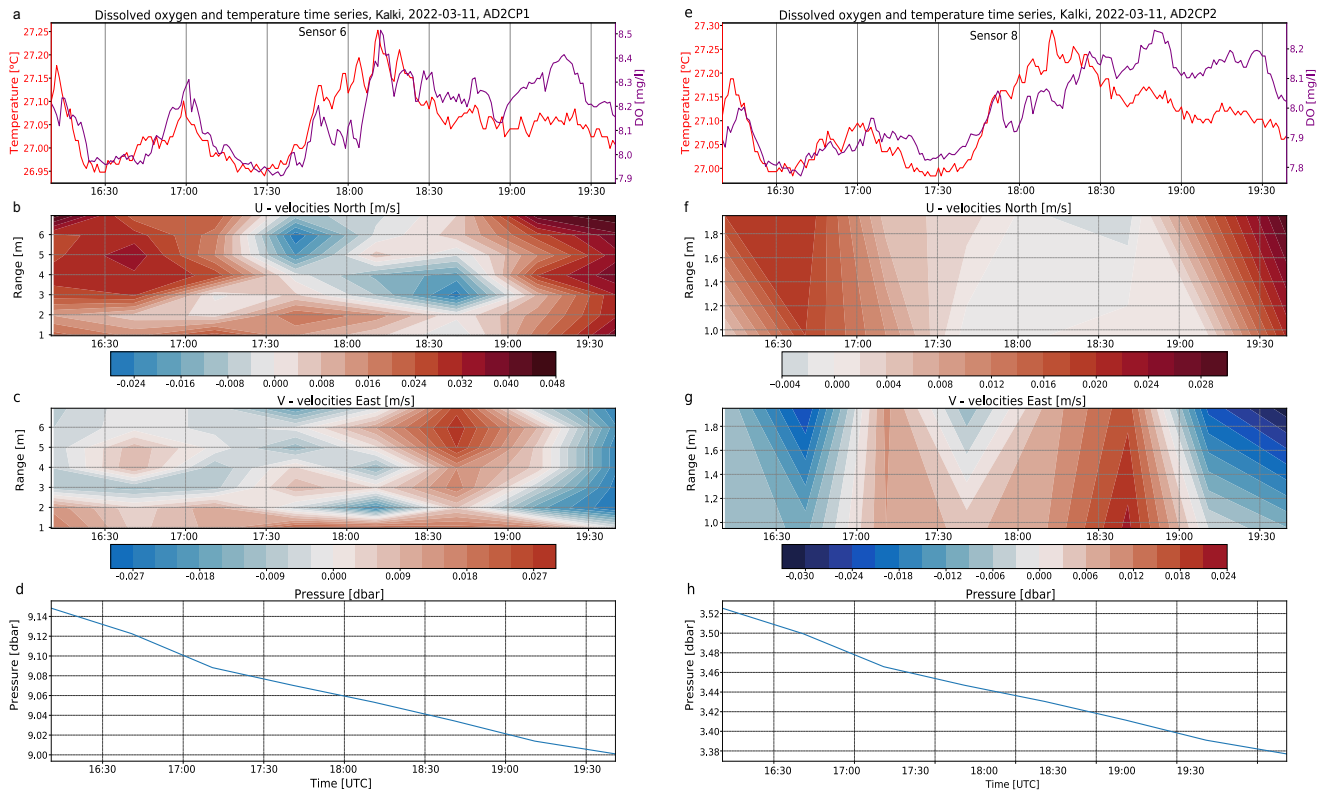


Figure 16: Field data from Kalki beach on March 11, 2022. AD2CP1 is on the left, AD2CP2 is on the right. From top to bottom: Dissolved oxygen (mg/L) and temperature (C), north velocity (m/s), east velocity (m/s), and water pressure (dbar)

## Director's Bay March 13, 2022

Figure 17 shows data from Director's Bay on March 13<sup>th</sup>. Only data from AD2CP1 was useable (to be discussed further in the discussion). Further details about the instrument deployment can be found in table 1 and Appendix A. Current velocities switched from north to south about halfway through the measurement period at the same time as the peak eastward velocity (.045 m/s). Northward currents were strongest in the top 1 meter from the surface, and gradually decreased towards the bottom. The pressure showed a transition from high tide to low tide (high pressure to low pressure, fig 17 d), and the switch from north to south flowing velocity happened in the middle of this transition (fig 17 b and d). No wave data was taken at this site.

The DO concentration followed a relatively consistent saw-tooth pattern throughout the entire time series (fig 17 a). DO peaked around 15:45 during the switch of velocity direction, when the northward velocity started to become weaker. This followed patterns that have been seen at other sites. There was an increase in DO around 15:00 that deviates from this pattern,

increasing during a period of strong velocity. Both AD2CPs showed a dominating north/south flow, with weaker flows in the east/west direction.

### Daaibooi March 15, 2022

Figure 18 shows the data from Daaibooi beach on March 15<sup>th</sup>. As seen in the data from this same site on March 23<sup>rd</sup> (fig 10), there was a quick switch from southward flow to northward, then back again. The period of northward velocity lasted an hour, from 16:30 to 17:30, and was seen at both AD2CP sites (closer to the shore and shallower, and further away and deeper). This transition happened during the change from high to low tide, as seen in the pressure plots (fig 18 d). Towards the end of the measurement period, there was an increase in southward velocity in the surface and the top 2 meters. No wave data was taken on this date.

The DO from both sensors differed greatly, until 17:30, when they followed a very similar pattern (fig 18 a). At both locations, there was a decrease in DO during the last switch from north to south velocity. This decrease happened during extremely weak flow (close to 0.0 m/s), followed by an increase as velocity increased in the south direction. Sensor 6 showed a higher overall DO concentration than sensor 8, with less extreme variability in values.

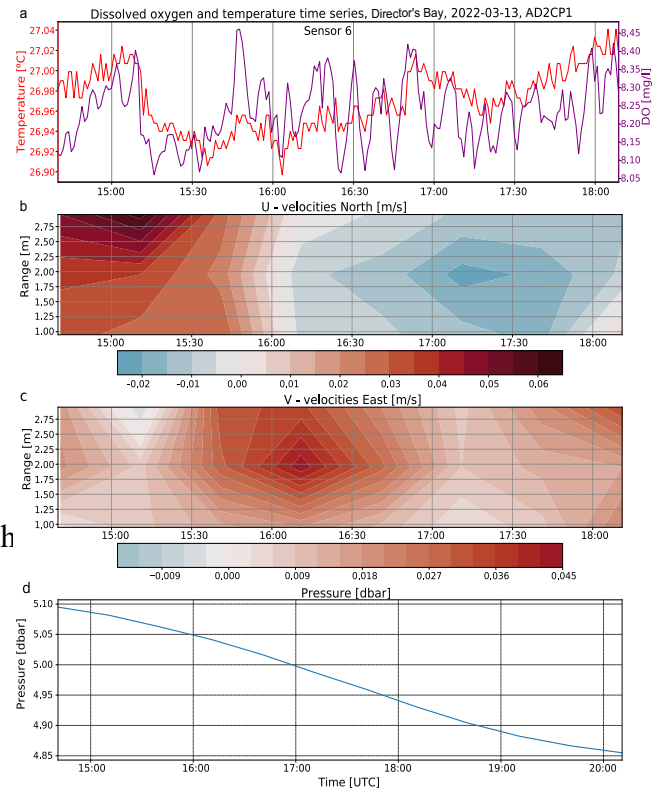


Figure 17: AD2CP and miniDOT logger data from March 13, 2022 at Director's Bay. From top to bottom: Dissolved oxygen (mg/L) and temperature (°C), north velocity (m/s), and east velocity (m/s). The right graphs are from AD2CP1 and the left are from AD2CP2

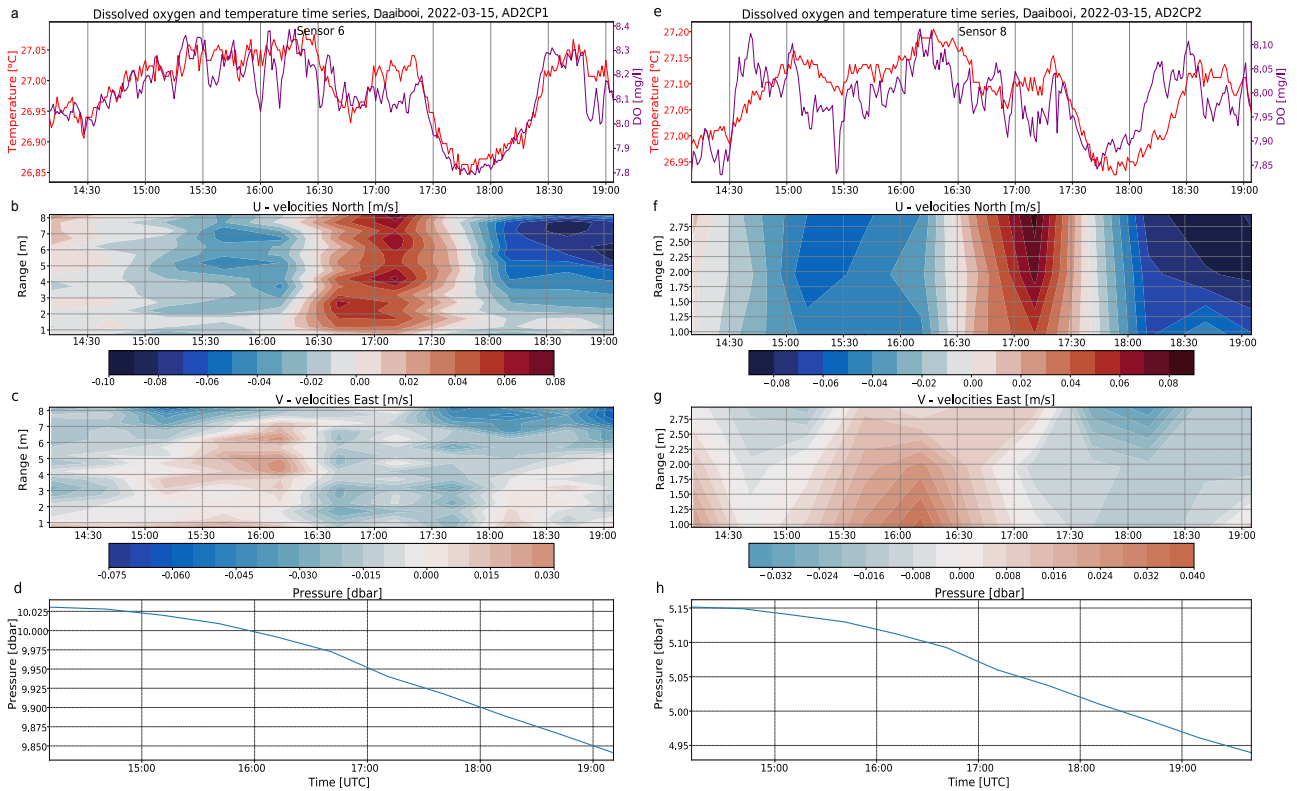


Figure 18: Field data from Daaibooi beach on March 15, 2022. AD2CP1 is on the left, AD2CP2 is on the right. From top to bottom: Dissolved oxygen (mg/L) and temperature (C), north velocity (m/s., east velocity (m/s), and water pressure (dbar)

### Piscadera Bay March 17, 2022

Figure 19 shows the field data from Piscadera Bay on March 17<sup>th</sup>. Both AD2CPs showed very similar velocity profiles, even though AD2CP2 was at a much shallower depth close to shore. For the first hour, the current flowed in the southeast direction, then switched to a northwest direction for the rest of the time series. This switch happened right around the transition period from low to high tide (fig 19 e and j). The eastern flow was much stronger in the AD2CP1 data (.04 m/s) compared to AD2CP2 (.008 m/s). Current velocities for both AD2CPs were stronger in the top 1 meter of measurement. The wave height data for AD2CP1 showed a peak wave height of .7 m towards the end of the measurement period, coinciding with the peak north current velocity around 18:45 (fig 19 b and g). The wave height for AD2CP2 fluctuated very little, from .48 m to .59 m, with a peak of .59 m.

DO for sensor 6 showed a peak around 14:30, during the period of very weak velocity, followed by a decrease as velocity increases (fig 19 a and f). Both sensors showed a decrease in DO around the same time as the peak north velocity for both AD2CPs.

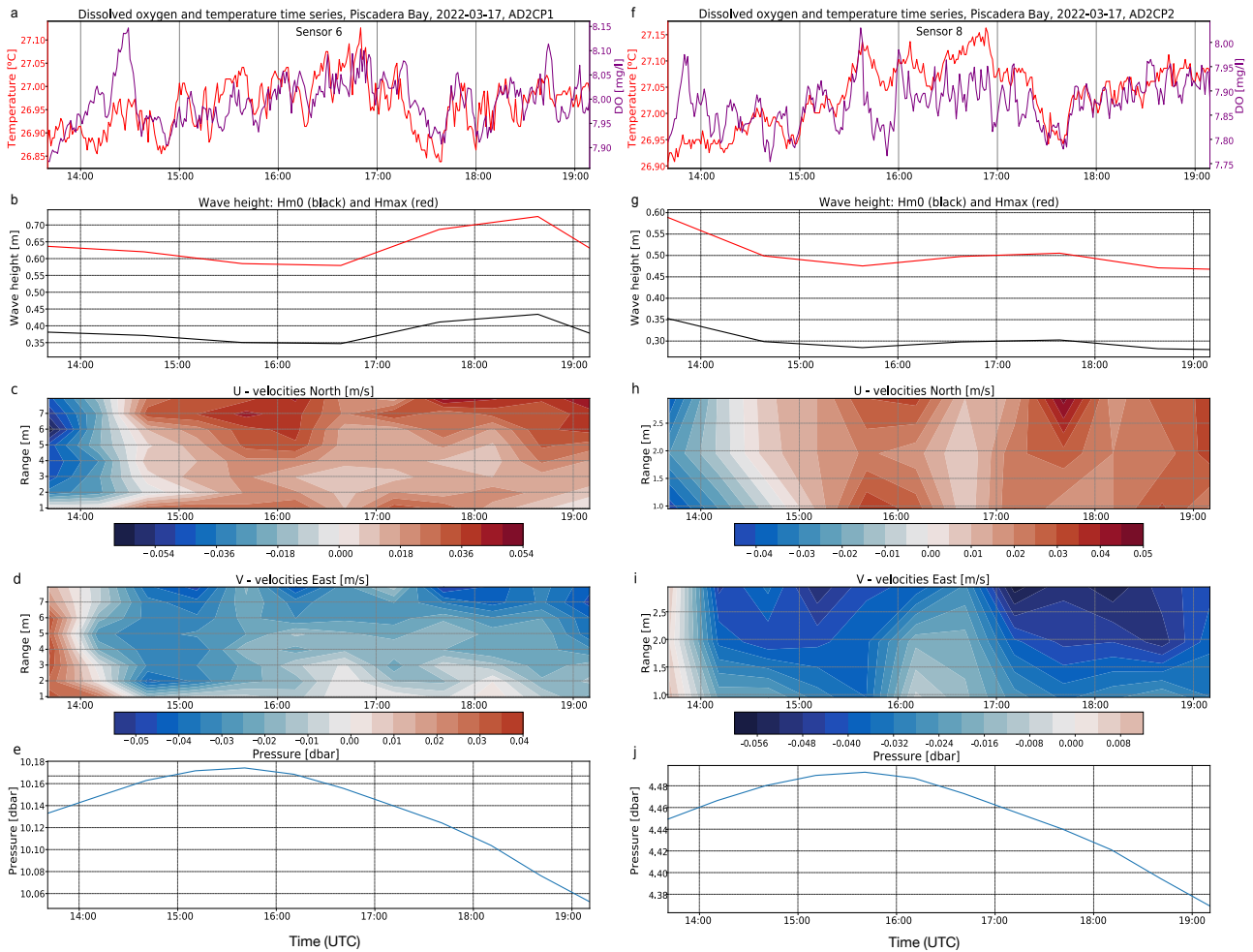


Figure 19: Field data from Piscadera Bay on March 17, 2022. AD2CP1 is on the left, AD2CP2 is on the right. From top to bottom: Dissolved oxygen (mg/L) and temperature (C), wave height (m), north velocity (m/s., east velocity (m/s), and water pressure (dbar)

### Director’s Bay March 28, 2022

Figure 20 shows the field data for Director’s Bay on March 28<sup>th</sup>. Both AD2CPs showed a southwards flow, but AD2CP1 showed two periods of stronger northwards flow on the surface, with a strong west component during the first instance (fig 20 c-d). There was a very strong southern flow shown in both AD2CPs at the end of the measurement period. The tide was in a transition period of low to high tide for the first 1.5 hours, then transitioned from high to low tide for the rest of the measurement period (fig 20 e and j). The maximum wave heights varied between .45 m and .75 m for both AD2CPs, with a peak wave height shown at 17:45 (fig b and g).

Each increase in wave height corresponded to a decrease in DO (fig 20 b and g). Sensor 6 varied between 7.85 mg/L and 8.32 mg/L while sensor 8 varied between 7.65 mg/L and 8.1 mg/L (fig 20 a and f).

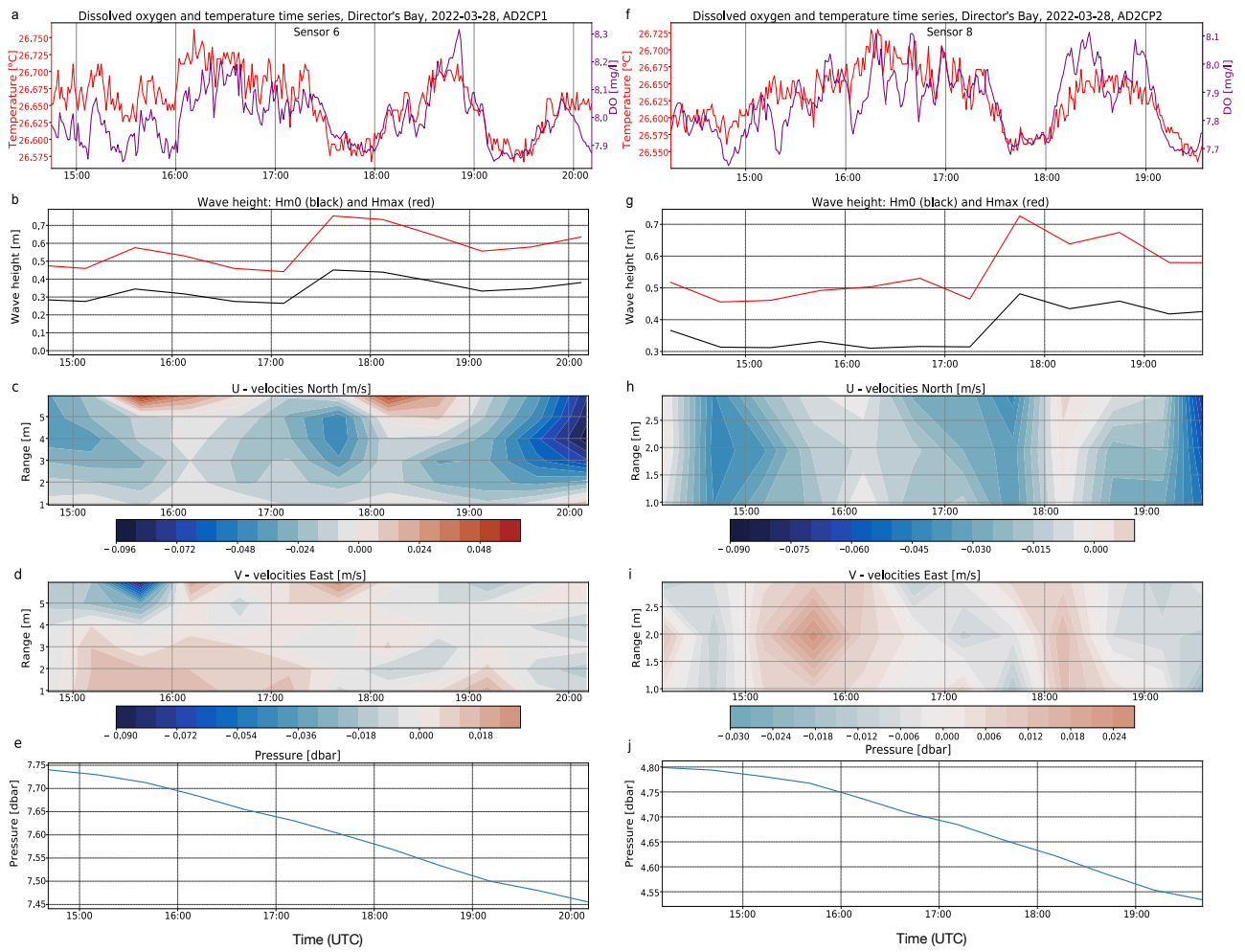


Figure 20: Field data from Director's Bay on March 28, 2022. AD2CP1 is on the left, AD2CP2 is on the right. From top to bottom: Dissolved oxygen (mg/L) and temperature (C), wave height (m), north velocity (m/s), east velocity (m/s), and water pressure (dbar)

### 4.1.3 Cross-shore vs along-shore

We were able to collect cross-shore data and along-shore data for Boca Sami on March 20, 2022 (cross-shore) and March 30, 2022 (along-shore). For March 20, AD2CP1 was set up according to plan F and AD2CP2 was set up according to plan G (table 1, appendix A). For March 30, AD2CP1 was set up following plan F and AD2CP2 was set up following plan H (table 1, appendix A). Figure 20 shows the cross-shore current data for March 20. The velocity was mainly flowing southeast for the entire data collection period (6 hours), with a quick switch to northeast around 18:45 for AD2CP1 (fig 21 a-b, 21 b; further offshore, at 8 m depth), and around 18:00 for AD2CP2, which was near-shore at 3.25 m depth (fig 21 c-d). The southward velocities from offshore were overall stronger than near-shore velocities, with an apparent velocity gradient that decreased from the surface down to the bottom. Both AD2CPs showed a peak eastward velocity around 18:00, while the near-shore AD2CP2 showed another period of strong eastward flow between 1.25 m and 2.25 m at the end of the collection period. This data was taken during neap tide, when the tidal range was smaller.

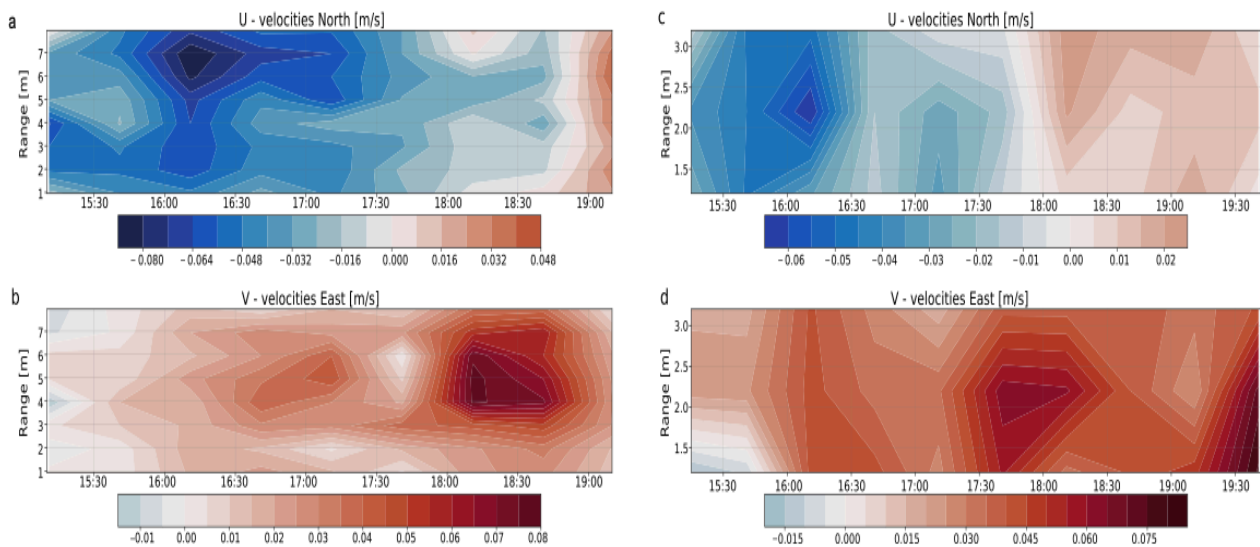


Figure 21: Cross-shore velocity data from Boca Sami on March 20, 2022. A-b are from AD2CP1 and c-d are from AD2CP2.

The along-shore data, shown in figure 22, was taken 10 days later in approximately the same spot as the off-shore AD2CP1, at 8 m depth (fig 22 a-b). Both AD2CPs showed an initial southward flowing velocity at the beginning of the collection period, that then switched to a strong northward velocity for the next 5.5 hours before switching directions again to south for the duration of the data collection period. AD2CP1 recorded an eastward flow for the first hour before it switched direction, but showed an extremely low velocity, close to zero. Both

AD2CPs recorded depth variations in velocity, including a very slow-moving eastward velocity between 6 and 7 meters during the last 3 hours, and an hour-long period (between 17:15 and 18:15) of westward flow between 1 and 2 meters. AD2CP2 (fig 22 c-d) recorded a stronger northwards velocity extending throughout the length of the measurement depth between 14:30 and 16:00. The data taken this day was during spring tide, when the tidal range is very large.

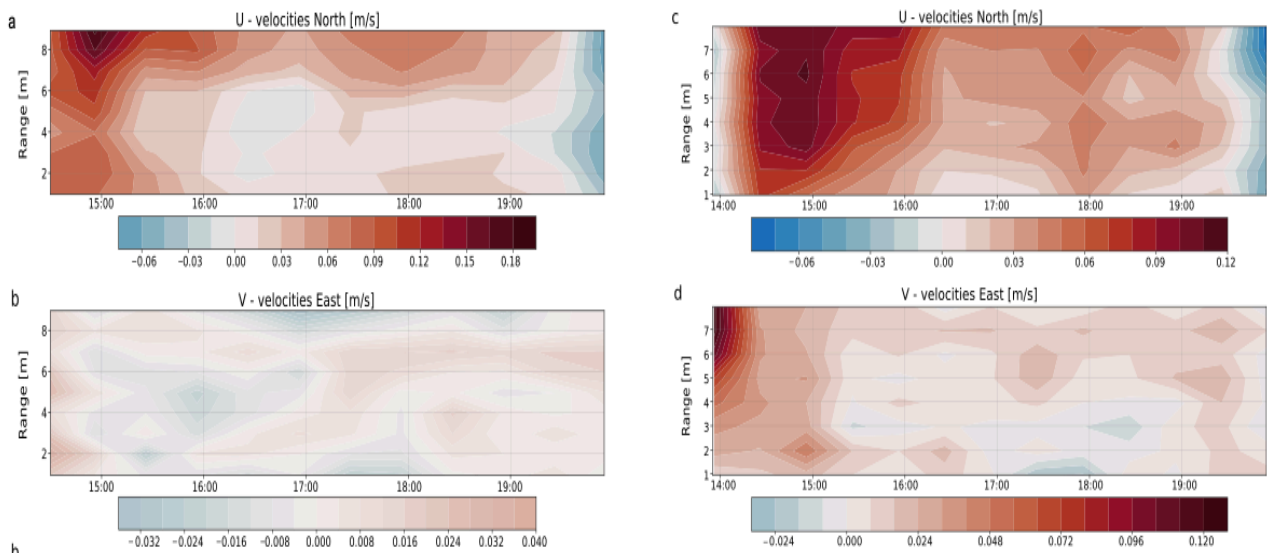


Figure 22: Along-shore velocity data from Boca Sami on March 30, 2022. A-b are from AD2CP1 and c-d are from AD2CP2

The wave heights for the cross-shore and along-shore data varied a lot over time and are shown in figure 23. AD2CP1 (offshore) had an average maximum wave height of about .5 meters, while the near-shore data showed it to be closer to .3 meters (fig 23 a and c). This could indicate that the waves broke while propagating towards the coastline. AD2CP1 recorded an increase in the max wave height at 18:45 that did not show on the AD2CP2 data. The along-shore data set (fig 23 b and d) showed more variations in wave height, and showed a gradual increase in average maximum wave height over time.

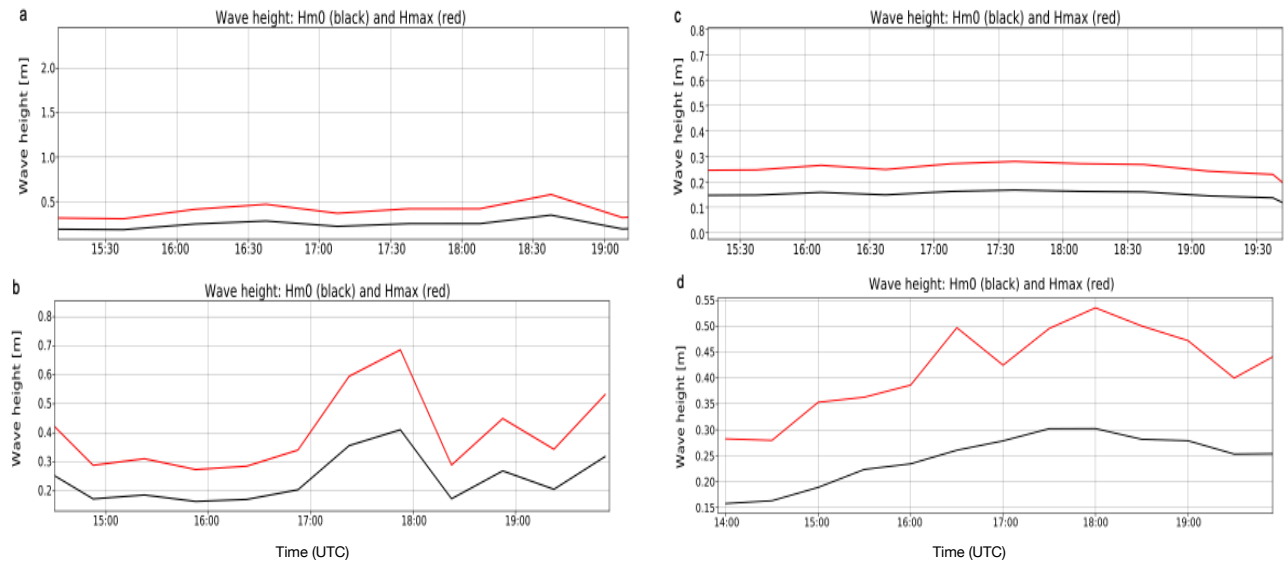


Figure 23: Maximum wave height (red) and significant wave height (black) for Boca Sami. AD2CP1 is on the right, AD2CP2 is on the left. A-b are from AD2CP1 and c-d are from AD2CP2. The top plots are from March 20 (cross-shore), while the bottom are from March 30 (along-shore).

For the cross-shore configuration shown in figure 24, dissolved oxygen concentrations from the loggers near AD2CP1 (fig 24 a; sensor 6) and AD2CP2 (fig 24 c; sensor 8) were quite similar, with an initial and steady increase for the first hour of measurements, followed by a sharp 15-minute decrease. This decrease could be the result of an increase in the southeastern current around 15:30, shown in the cross-shore current velocity plot in figure 10. The DO concentration increased after the sudden decrease for about a half hour, from 15:45-16:15, before decreasing again and staying at a lower concentration for the rest of the measurement period.

The along-shore DO data taken 10 days later (fig 24 b, 24 d) showed a very different trend. In both sensor 6 and 8, the DO appeared to increase and decrease in waves, more prominently seen in sensor 6. For sensor 6 (fig 24 b), the DO concentration steadily increased for the first 2.5 hours before decreasing briefly, then increased again for an hour before decreasing again. This trend appears to follow the maximum wave height trend of AD2CP1 (fig 23 b), with a decrease of DO coinciding with an increase in wave height maximum. The same trend can be seen with the wave height from AD2CP2 (fig 23 d) and the sensor 8 DO data trendline (fig 24).

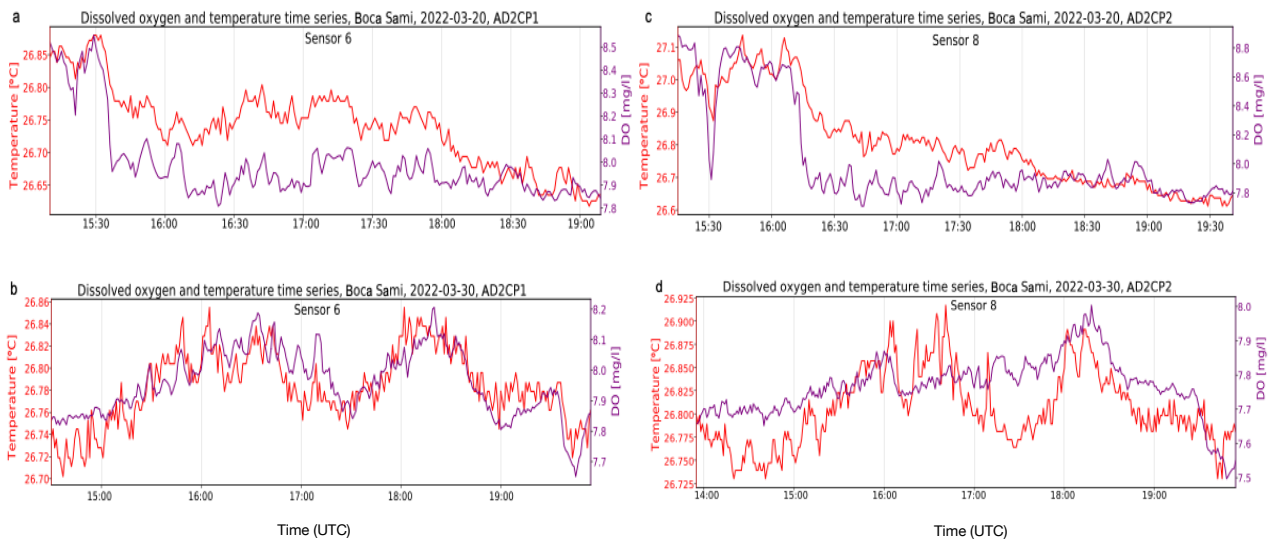


Figure 24: DO concentrations and temperature from Boca Sami on March 20 (top plots) and March 30 (bottom plots). The left plots (a-b; sensor 6) are from the logger near AD2CP1, and the right plots (c-d; sensor 8) are from the logger near AD2CP2. Dissolved oxygen (mg/L) is in purple and temperature (C) is in red.

## Speed and direction for all locations

Figure 25 displays the average speed and direction per location, for all measurement days, while figure 26 displays the same but for de-trended data (the tidal trend and seasonality has been removed), i.e., residual current. The speed ranges are dictated by different colors, while the size of the color bars represents how often the current was in each range. The rings in the plots represent the percentage of the total time spent flowing in a single direction, and each slice shows how long the current flowed in that specific direction.

It is clear in figure 25 that the speed and direction of currents depends heavily on location. East Point and Director's Bay, although in close proximity on the island, were vastly different. Currents at both locations appeared to flow along-shore, but in opposite directions. The current at East Point was flowing west-northwest for 9% of the time, northwest for 7% of the time, and north-northwest for 8% of the time, with a peak direction in the west-northwest direction. The current speeds varied between .01 and .30 m/s. At Director's Bay, the peak current was east-southeast (8% of the total time), followed by east (7.2 %) and southeast (7%), and the current speed was between .00 and .06 m/s. Piscadera Bay current direction was primarily northwards and along-shore, with a range between .01 and .10 m/s in all directions. Boca Sami had the most consistent range, hovering between .05 and .10 m/s in the west to north directions most of the time. The peak directions were north and northwest (both 14% of the time), followed by north-northwest (12% of the time).

Daaibooi was the most variable, with peak directions of south-southeast and northwest (along-shore flowing), at a slower speed compared to the previous locations. The current flowed in all directions for at least 2% of the total time. Cas Abao was dominated by a northwest flow for 14% of the time at speeds between .01 and .10 m/s, in an along-shore direction. Kalki, located close to the west point of the island, was dominated by maximum current speeds of .06 m/s in almost all directions. The peak direction, west, was dominated by currents of .03 m/s. Flow was mainly cross-shore, primarily in the offshore direction.

The data was then de-trended and the residual currents were then used in order to identify the impact of the tides and seasonality on the results from figure 25 (shown in figure 26). The most imperative result from these plots is that the tidal component is extremely important to dictating current speed and direction. The biggest differences can be seen in East Point,

Director's Bay, Cas Abao, and Kalki, where the currents would flow in a cross-shore direction. Without the tidal component, East Point currents would be almost one order of magnitude slower (.02-.04 m/s) and flow north towards the coast, Director's Bay would flow primarily north, Cas Abao currents would flow northeast, and Kalki would flow north. The current speed in all location was between .00 and .04 m/s maximum. The residual currents point towards the shore in all locations, which is in agreement with the direction of the wind in the wind rose plot (fig 1).

ADCP measurements, March 2022: bottom currents

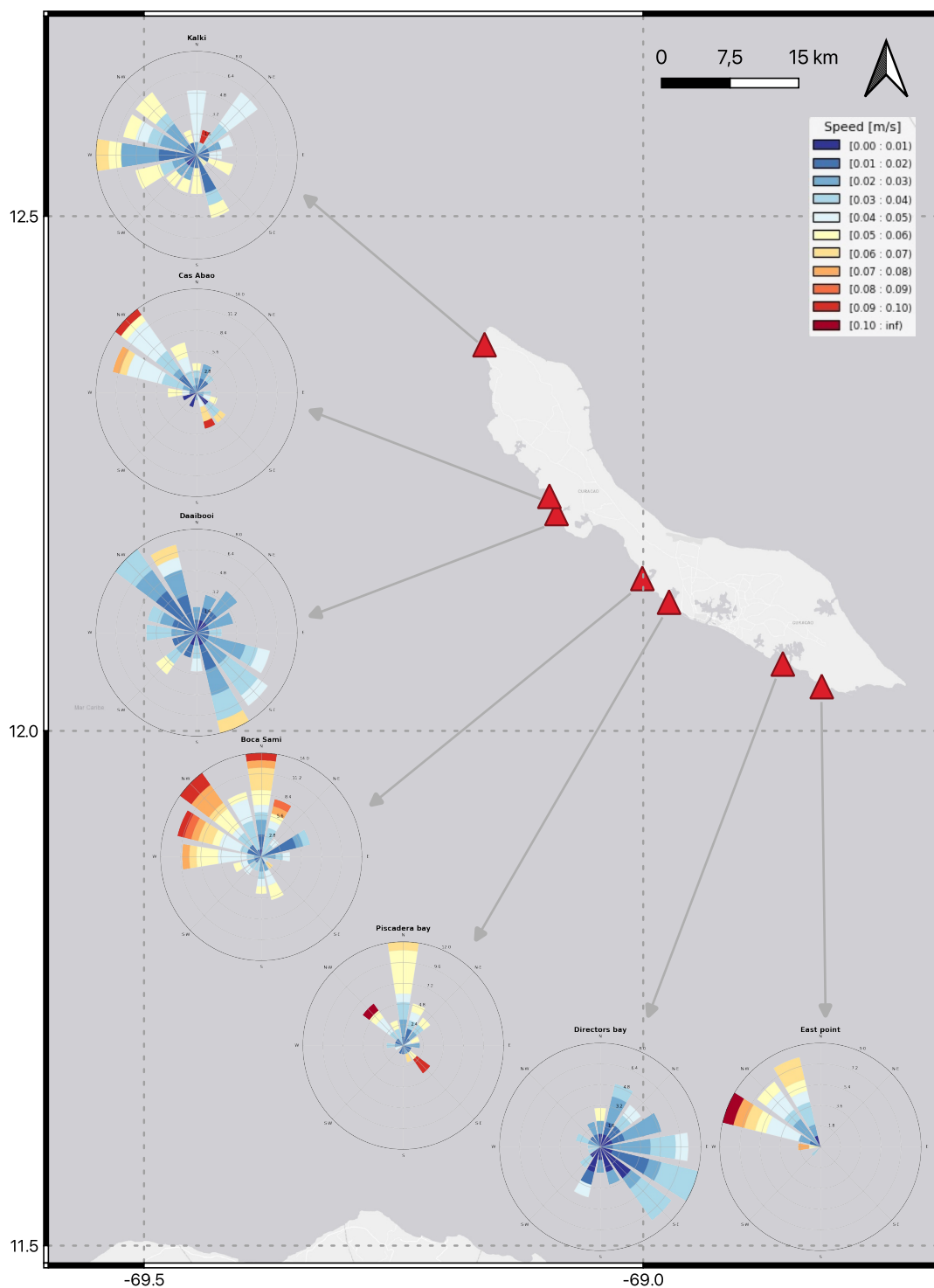


Figure 25: Average speed and direction for all study locations. Color bars represent speed range.

ADCP measurements, March 2022: bottom currents - residual

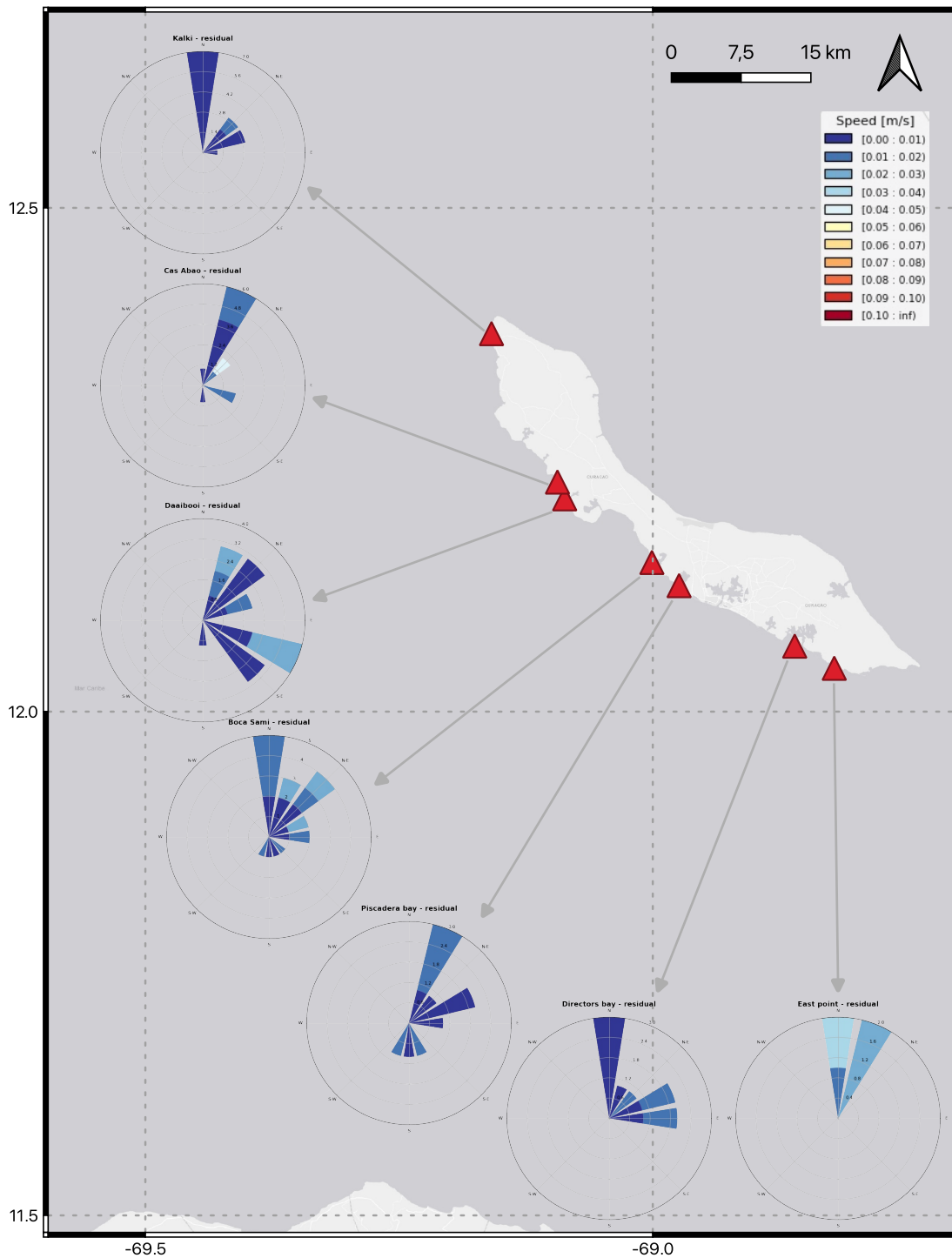


Figure 26: Average speed and direction for all study locations, with no tidal component or seasonality. Color bars represent speed range.



The east bottom velocity values, located .95 m above the sea floor, were used as a predictor value for DO in the Granger causality test. There were 3 locations and 4 days where the east velocity was found to be a predictor for DO (fig 28 a-b). Both dates at Daaibooi beach, March 15<sup>th</sup>, and March 23<sup>rd</sup>, showed that lag 2 can be used. March 15<sup>th</sup> showed that lag 3 could also be used (fig 28 a). Different from the north velocities, Cas Abao on April 1<sup>st</sup> showed a causation for east bottom velocities, but no causation on March 29<sup>th</sup>. On March 20<sup>th</sup>, the values from Boca Sami showed a causation for almost all five time lags, except for the first lag (fig 28 a). This shows that the east bottom velocities can be used to predict the DO values recorded for that day.

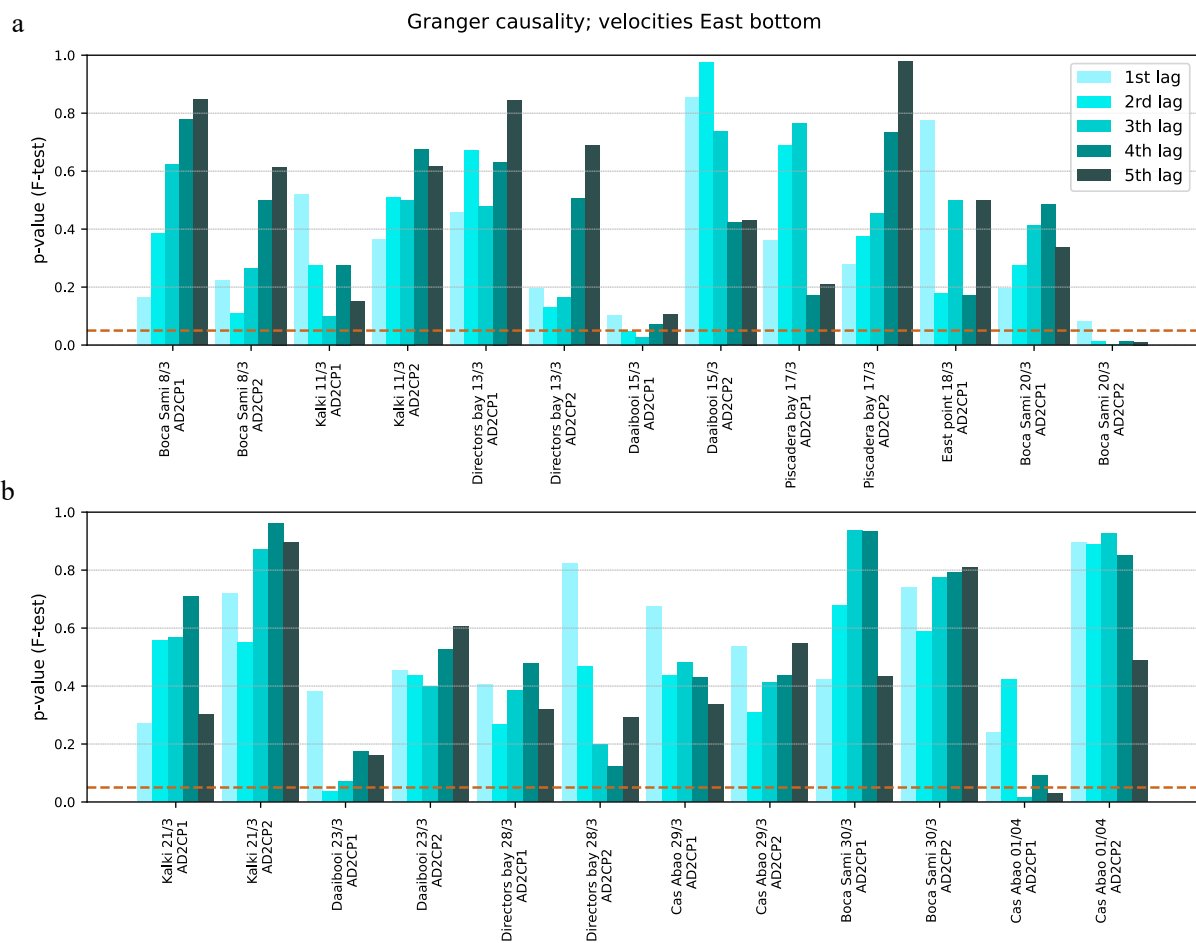


Figure 28: Granger Causality test using east bottom velocity as a predictor for DO concentration. All study locations and dates are present. Each lag represents a delay in time of 10 minutes. The p-value threshold of .05 is marked by the red dotted horizontal line.

## 4.2 Model findings

The Granger Causality tests show that velocity is not the primary cause of the DO patterns seen in our field data, and that other oceanic processes contribute to DO fluctuations.

Understanding additional factors that can influence DO concentration around coral reefs is key to a broader understanding of variables that can impact reef health. Other parameters, in conjunction with velocity, likely caused these patterns. Oxygen diffusion and water viscosity (how “thick” a liquid is) are known to influence water oxygen distribution and water flow (Finelli et al., 2006). In order to test these parameters and their impact on oxygen concentration, oxygen diffusion and seawater viscosity values typically seen in natural environments ([engineeringtoolbox.com](http://engineeringtoolbox.com)) and in situ north bottom velocity values from Boca Sami on March 8<sup>th</sup> were used in a CFD model. The north bottom velocity values were used because the Granger test showed the most causality between north bottom velocity values and DO. This model was created in order to help us gain insight into the flow around coral reefs and the resulting movement of oxygen. A model allows us to ignore, or “switch off”, other processes that occur in the ocean, such as waves and biological processes, in order to focus on a specific factor of interest (diffusion and viscosity in this case) and to test the extent of a relationship between factors.

Four simulations were run with the time-interpolated field data velocity values. For the modelled environment (one coral), two simulations were run with a constant oxygen diffusion value of  $9 \times 10^{-8} \text{ m}^2/\text{s}$ , and differing water viscosity values (S1 and S2), and two were run with a constant water viscosity value of  $9 \times 10^{-4} \text{ Pa}\cdot\text{s}$ , and differing oxygen diffusion values (S3 and S4). These simulations had time limitations for the model to successfully run, potentially preventing a visualization of the full process. Stationary, i.e. not time-dependent, simulations of S1-S4 were run in order to be able to visualize the influence of diffusion and viscosity on dissolved oxygen.

A final time-dependent simulation was run with a fixed water viscosity and oxygen diffusion and constant velocity that switched direction halfway through the simulation. The fixed viscosity was chosen as  $9 \times 10^{-4} \text{ Pa}\cdot\text{s}$  (the typical viscosity value of oxygen in seawater at

27°C) and diffusion as  $9 \times 10^{-8} \text{ m}^2/\text{s}$ . This was done to mimic the change in velocity direction seen at the end of the data from Boca Sami on March 8<sup>th</sup> (fig 15).

### Influence of Viscosity

The results from S1 and S2 are shown in figures 29 and 30. Two time points were chosen: when the oxygen reaches the right side of the coral and when the simulation ended. S1 had a higher viscosity value of  $1 \times 10^{-3} \text{ Pa}\cdot\text{s}$  (the typically measured viscosity of oxygen in seawater at 0°C), and S2 used a lower value of  $9 \times 10^{-4} \text{ Pa}\cdot\text{s}$ . The biggest change between the two can be seen at the 677.9 s time point (fig 29 and 30 top plots) to the right of the coral. There is a lower concentration in the developing “shadow zone”, or a zone of low to zero oxygen, in S1, likely due to the higher water viscosity. S2 shows a more distributed concentration at both time points.

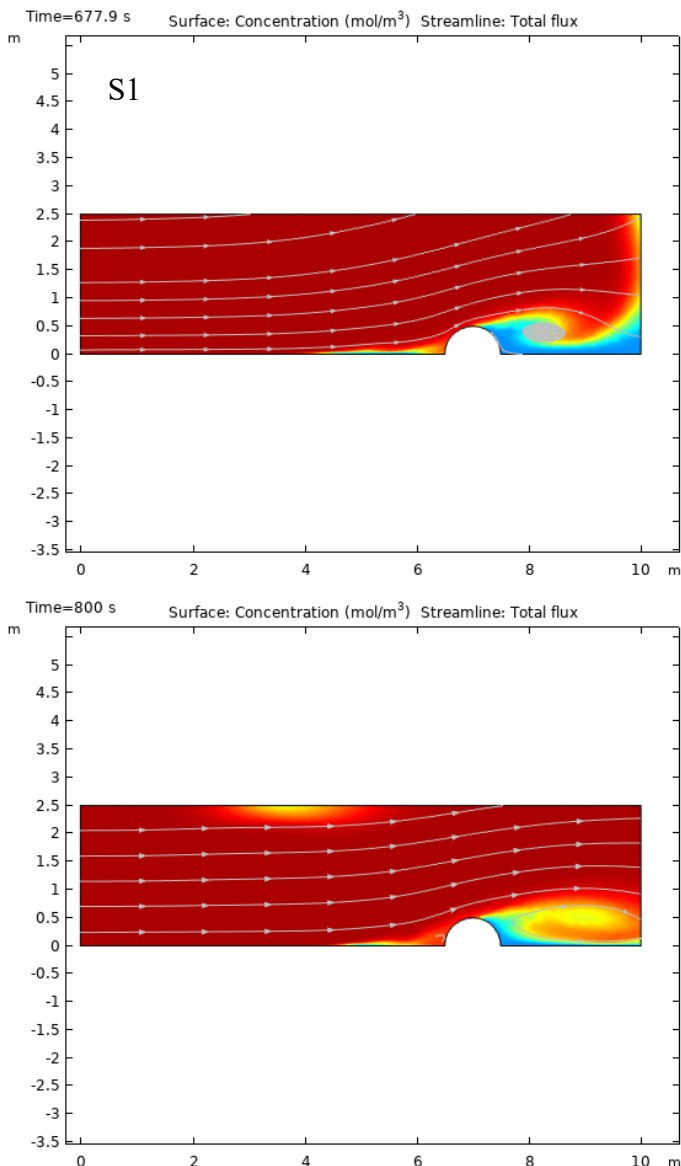


Figure 29: S1 oxygen concentration ( $\text{mol}/\text{m}^3$ ) at 677.9 s (top) and at the end of the simulation (800 s; bottom). The color bar on the left shows the velocity values, and the x and y axes show height and length in meters

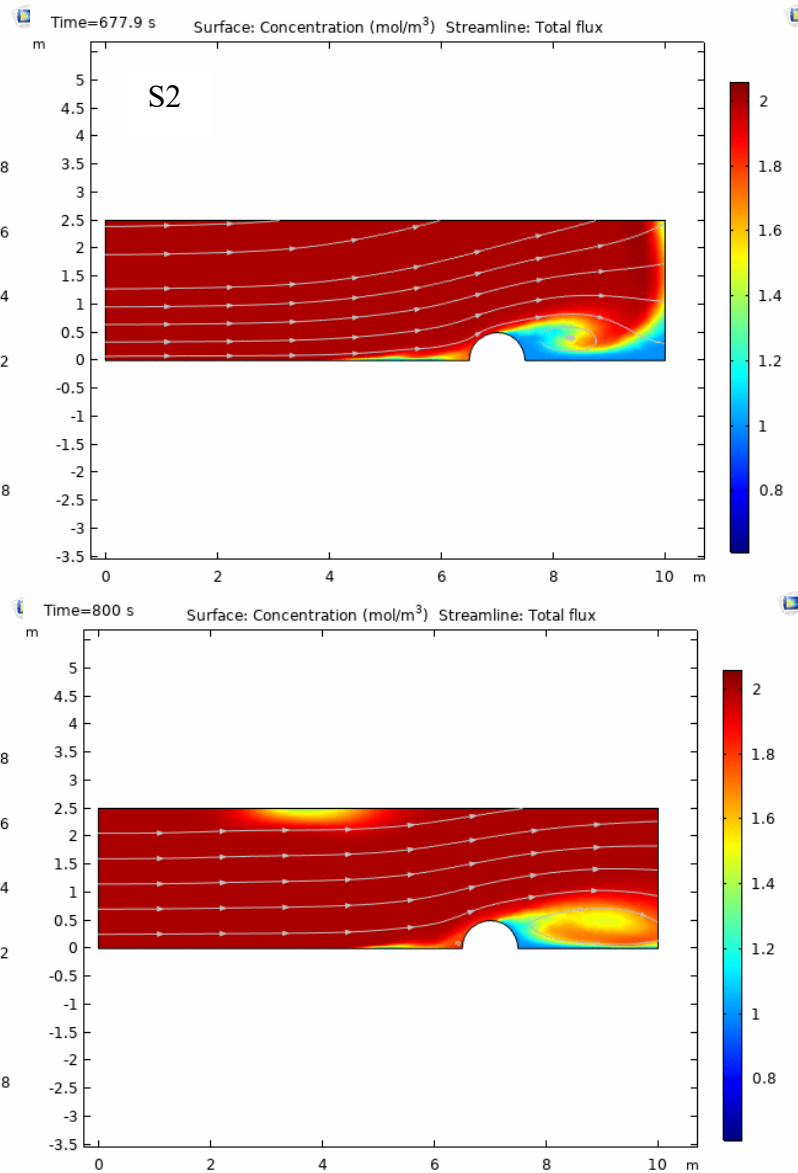


Figure 30: S2 oxygen concentration ( $\text{mol}/\text{m}^3$ ) at 677.9 s (top) and at the end of the simulation (800 s; bottom). The color bar on the left shows the velocity values, and the x and y axes show height and length in meters

These changes can be seen in the velocity vs concentration plotted over depth, shown in figures 31 and 32 below. The plots show velocity vs concentration over depth to the left of the coral and to the right of the coral. The blue dashed line (left side of coral) and red dash-dot line (right-side of coral) are velocity and the green line with plus signs (left side of coral) and teal line with points (right-side of coral) are concentration. The bottom plots at time 800 s differ in concentration around depth .4 m, right around the start of the forming shadow zone, with a higher concentration seen in the simulation with a lower viscosity (S2, fig 32 bottom).

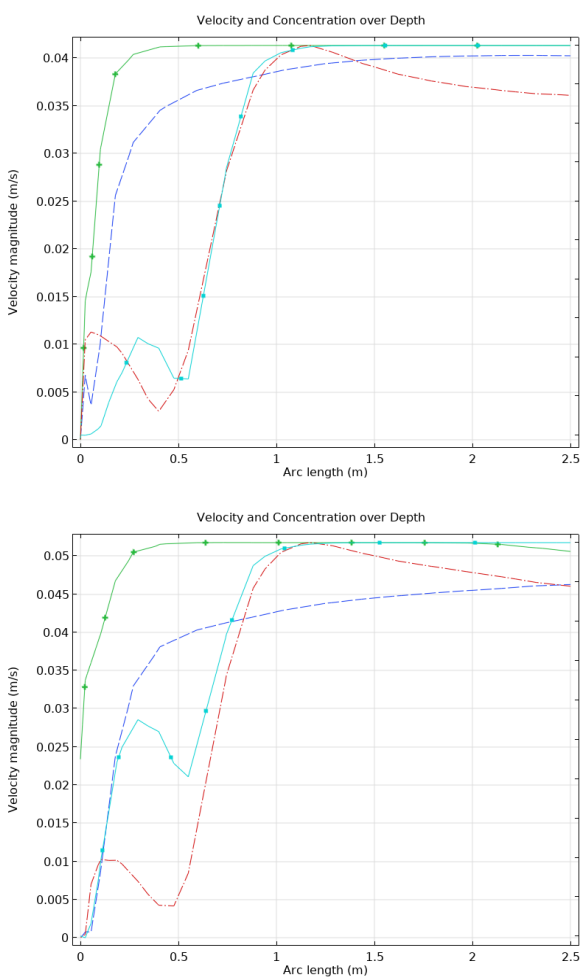


Figure 31: S1 velocity vs concentration over depth. Depth is labeled as "arc length" in the plots and shown in meters. The dashed lines are velocity, and the solid lines with markers are concentration

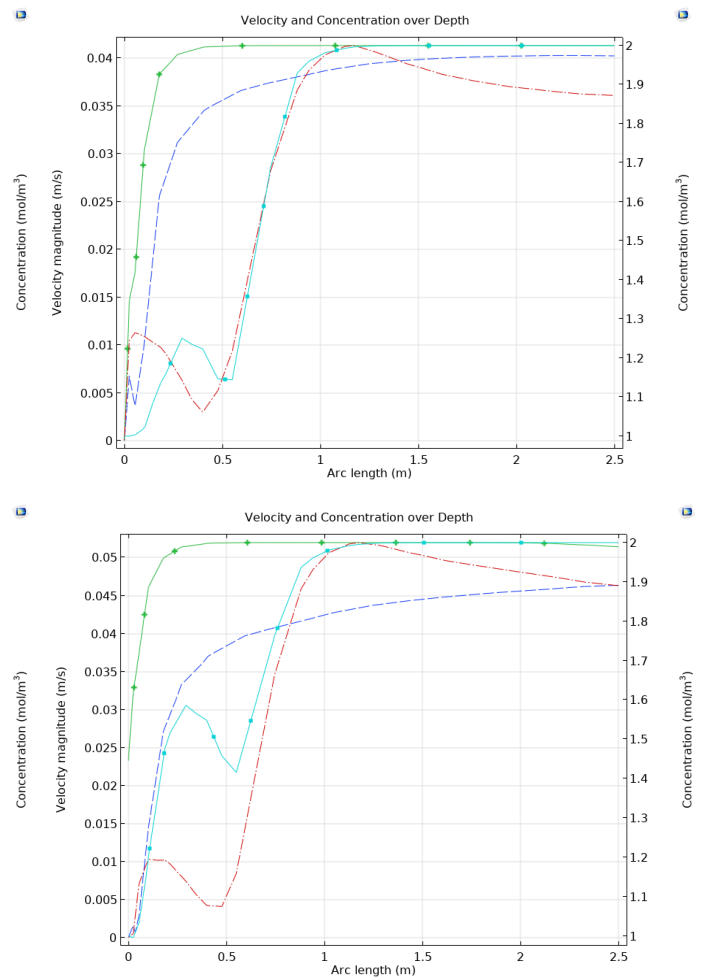


Figure 32: S2 velocity vs concentration over depth. Depth is labeled as "arc length" in the plots and shown in meters. The dashed lines are velocity, and the solid lines with markers are concentration

Figures 33 and 34 show the change in velocity and concentration over time, to the left and right of the coral. Both velocity and concentration are higher on the left side of the coral, which is consistent with the velocity and concentration depth plots (figures 31 and 32). The concentration to the right of the coral in S1 and S2 decreases after 600 s, and this can be seen in the top plots of figures 29 and 30. As the flow passes over the coral, part of it (and the oxygen with it) curls back towards the coral, creating a small vortex of a portion of the concentration, before it starts to increase again to equalize with the rest of the environment.

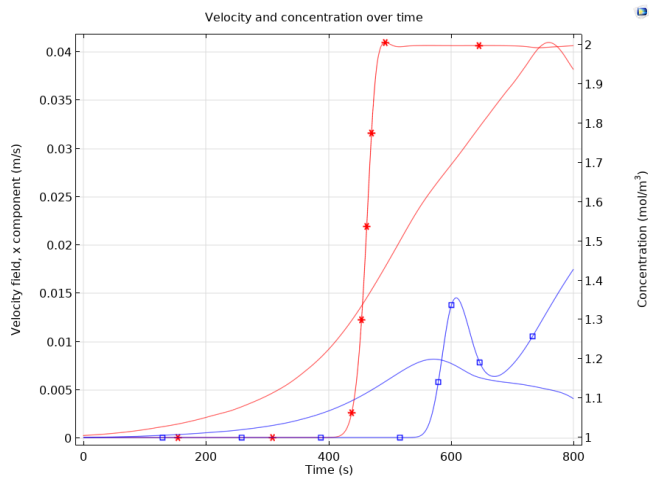


Figure 33: S1 Concentration and Velocity over time at two points: red is to the left of the coral, blue is to the right. Marked lines are concentration and solid are velocity.

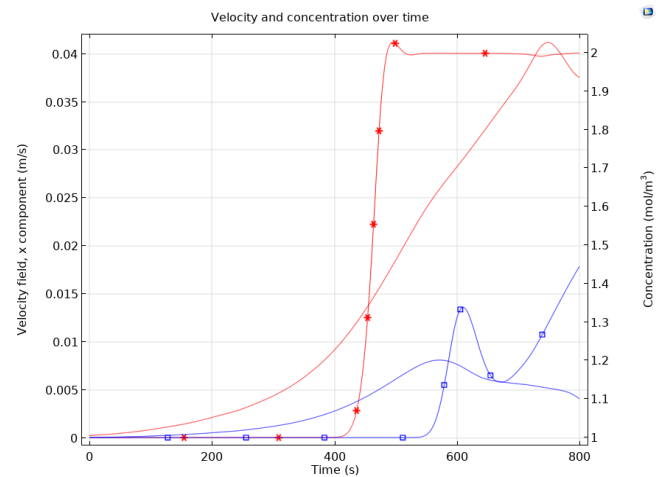


Figure 34: S2 Concentration and Velocity over time at two points: red is to the left of the coral, blue is to the right. Marked lines are concentration and solid are velocity.

### Influence of Diffusion

The results from S3 and S4 can be seen in figures 35 and 36, at the same time point as above, 677.9 s and 800 s. It is very clear that diffusion has a large impact on concentration. S4 has a larger diffusion value than S3, meaning that the oxygen will reach equilibrium more quickly (fig 34). The concentration in S4 is more mixed in the shadow zone to the right of the coral and the area to the left of the coral has nearly reached the equilibrium value of  $2 \text{ mol/m}^3$ . In the simulation with lower diffusion (S3, fig 35), there is a zone of close-to-zero concentration just to the left of the coral that is not seen with higher diffusion. In this case, the combination of viscosity and low diffusion could be causing this. The oxygen is being impacted heavily by two parameters in this case: diffusion and flow, causing it to disperse more quickly.

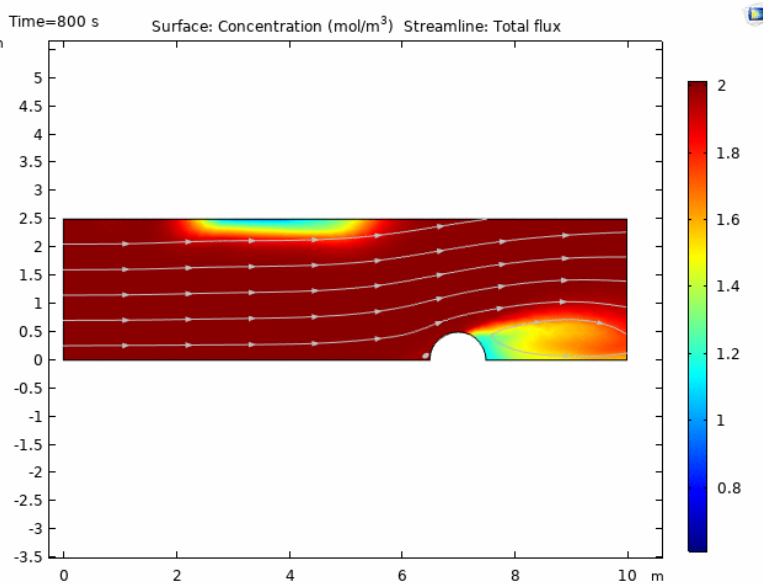
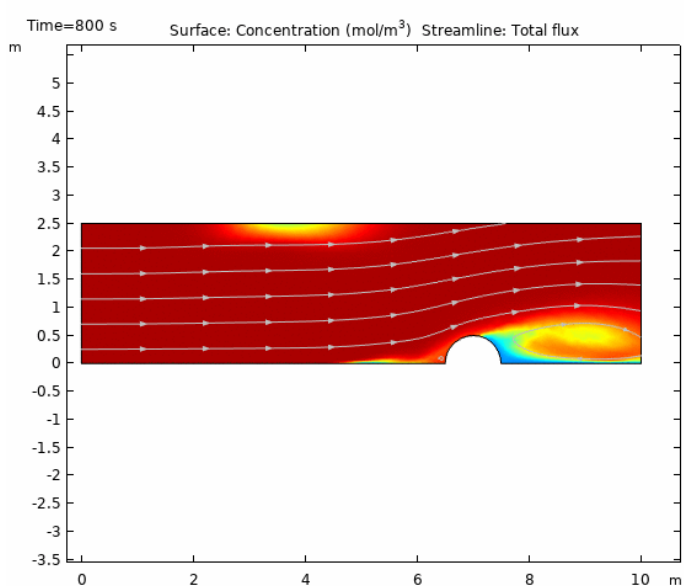
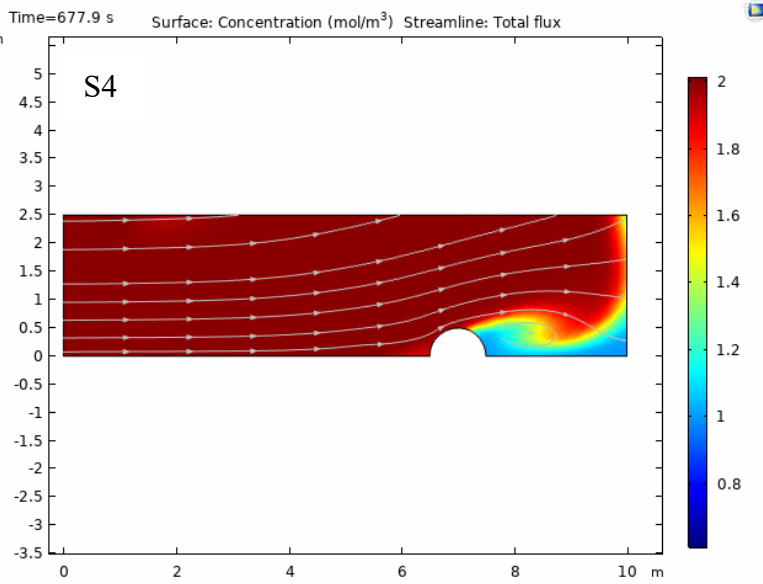
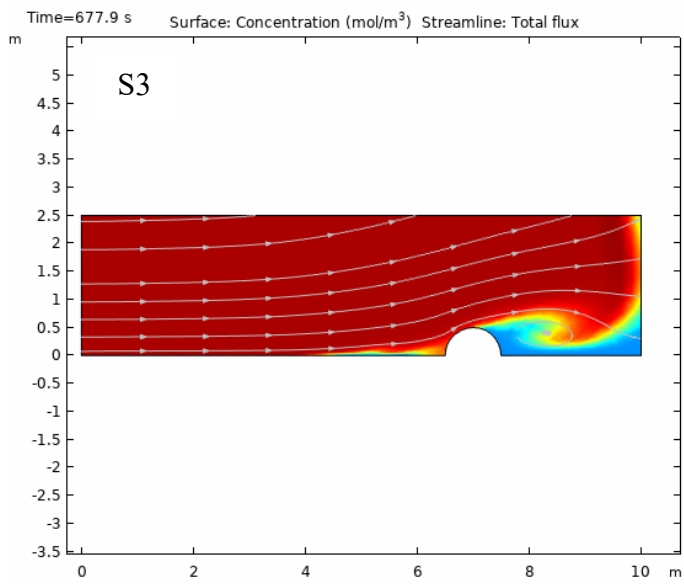


Figure 35: S3 concentration with close-to-zero diffusion. Color bar on the right shows concentration, x and y axes show height and depth in meters

Figure 36: S4 concentration with high diffusion. Color bar on the right shows concentration, x and y axes show height and depth in meters

Figures 37 and 38 show velocity vs concentration over depth for S3 and S4. The impact of diffusion on concentration, as described above, is very apparent in all the plots below, specifically in the plots for the right of the coral (teal line with markers). S3 shows a higher concentration over the first .6 meters of depth, while the concentration for S4 stays lower near the bottom.

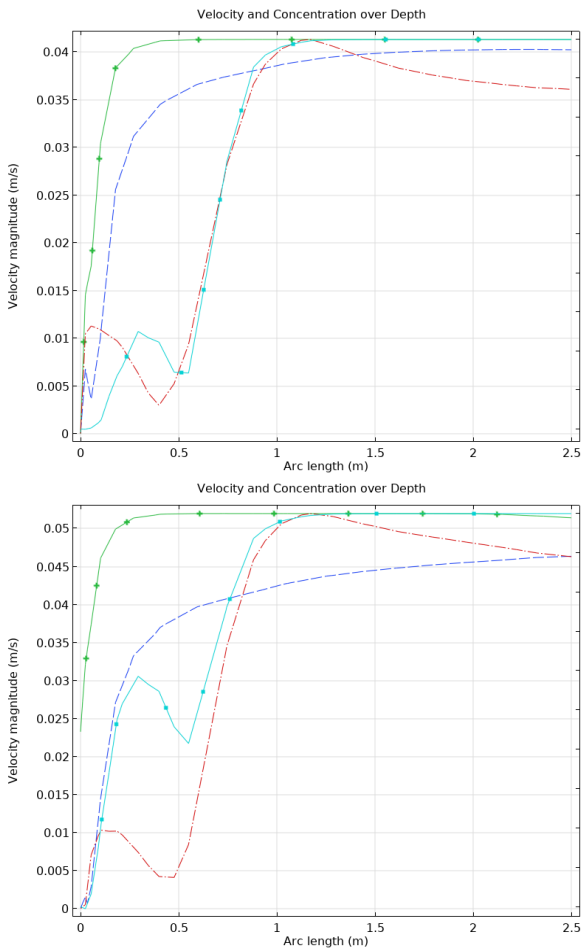


Figure 37: S3 velocity vs concentration over depth, at a low diffusion rate at time 677.9 s (top) and 800 s (bottom). Depth is labeled as "arc length" in the plots and shown in meters. The dashed lines are velocity, and the solid lines with markers are concentration

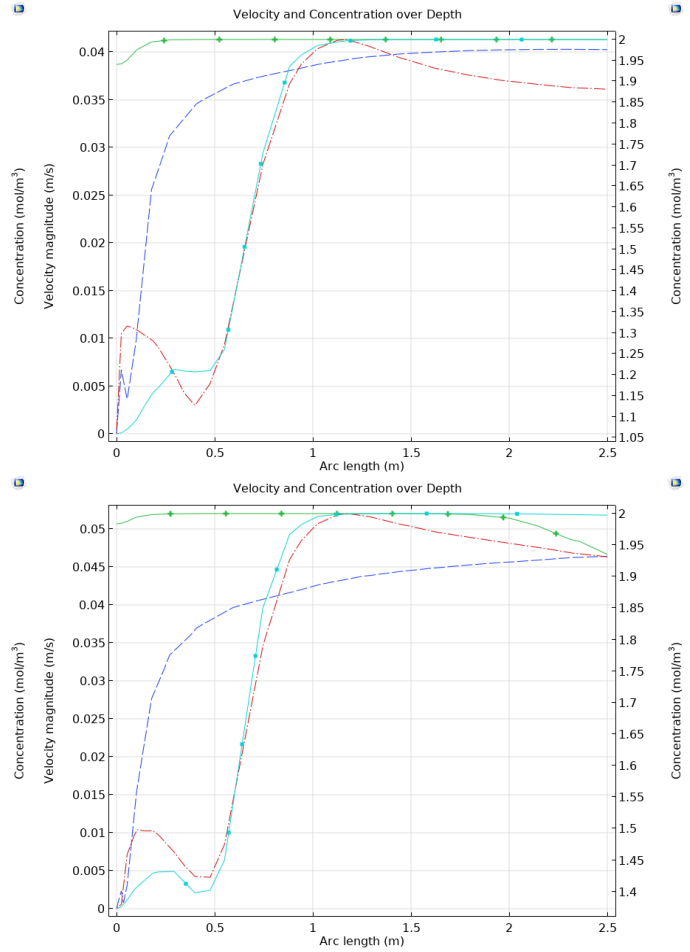


Figure 38: S4 velocity vs concentration over depth, at a low diffusion rate at time 677.9 s (top) and 800 s (bottom). Depth is labeled as "arc length" in the plots and shown in meters. The dashed lines are velocity, and the solid lines with markers are concentration

Figures 39 and 40 show the change of concentration and velocity over time to the left and right of the coral. The effect of diffusion can easily be seen in the concentration values, with the decrease during a lower diffusion rate (fig 39) much larger. As discussed in S2, a higher rate of diffusion results in the concentration going towards a state of equilibrium more quickly (fig 40).

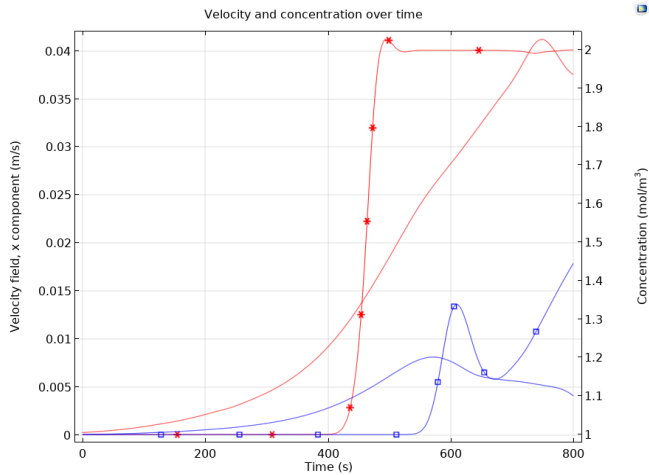


Figure 39: S3 Concentration and velocity over time at two points: red is to the left of the coral, blue is to the right. Marked lines are concentration and solid are velocity.

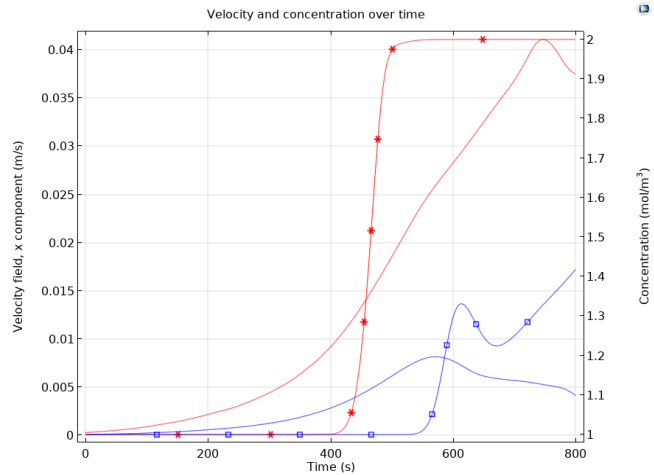


Figure 40: S4 Concentration and velocity over time at two points: red is to the left of the coral, blue is to the right. Marked lines are concentration and solid are velocity.

### Stationary simulations: Influence of viscosity

Figures 41 and 42 show the stationary results for S1 and S2 where the diffusion was kept constant but the viscosity value differed. There is a small zone of slightly lower concentration to the left of the coral in S1, possibly due to the higher viscosity (fig 41). The shadow zone on the left side of the coral is non-existent with a lower viscosity (fig 42), likely because the water flow and diffusion values were large enough to overcome the viscosity of the water, and disperse the oxygen more thoroughly throughout the simulation.

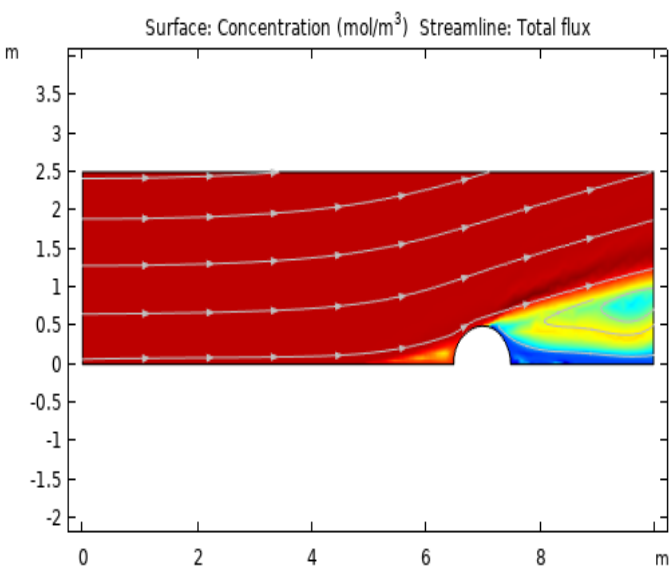


Figure 41: S1 Concentration with a higher viscosity value. The streamlines show the total flux of oxygen, and the color bar shows the concentration

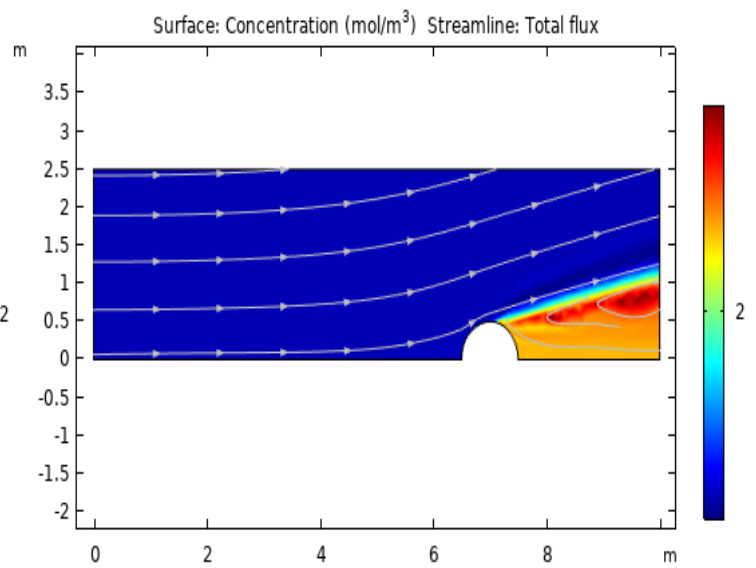


Figure 42: S2 Concentration with a lower viscosity value. The streamlines show the total flux of oxygen, and the color bar shows the concentration

### Stationary simulations: Influence of diffusion

Figures 43 and 44 show the stationary results for S3 and S4 where the viscosity was kept constant but the diffusion value differed. These plots show the high impact that diffusion has on oxygen concentration. At a high rate of diffusion (fig 39), the system has reached concentration equilibrium so there is no shadow zone or any areas of low or high concentration. This is unrealistic in the field due to the almost constant influx of oxygen into the water and a changing water flow. The DO plots in the field data results section show an always fluctuating concentration, never a constant value.

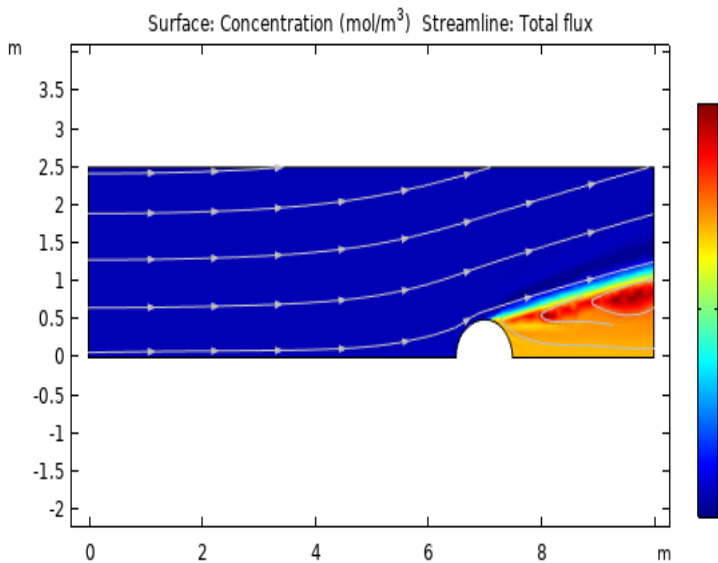


Figure 43: S3 Concentration with a lower diffusion rate. The color bar shows the concentration.

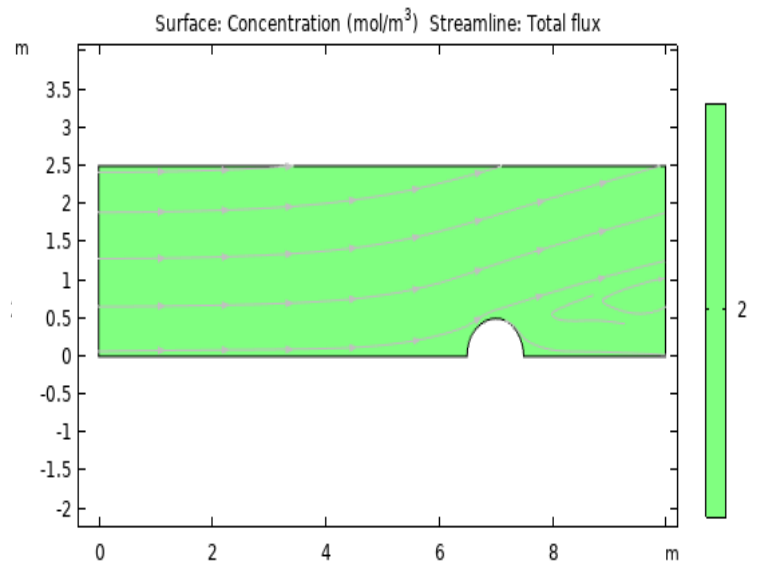


Figure 44: S4 Concentration with a higher diffusion rate. The color bar shows the concentration.

### **Velocity direction switch, constant viscosity and diffusion**

As a final test, the viscosity and diffusion were kept at constant values of  $9 \times 10^{-4} \text{ Pa}\cdot\text{s}$  and  $9 \times 10^{-8} \text{ m}^2/\text{s}$  respectively, while the velocity stayed at a fixed value of  $.01 \text{ m/s}$  for the first half of the simulation (normal flow), and then switched directions for the last half of the simulation, to  $-.01 \text{ m/s}$  (reverse flow). There was no new influx of concentration with the reverse flow, so all concentration seen in the simulation is residual from the normal flow. This velocity switch was seen in the field data towards the end of the measurement time at Boca Sami on March 8<sup>th</sup>. Figure 45 shows the results of chosen time points from the full time series, with the switch starting in the top right plot. The time series was run for a total of 3000 seconds in order to fully visualize the flow of oxygen in both directions.

With the sudden velocity direction switch, there is a first a small build-up of oxygen on the right side of the coral, that destroys the shadow zone (fig 45, top left). Residual concentration can be seen coming from the left of the box, and it interacts with the reverse flow. As the reverse flow becomes dominant, there is a new shadow zone that is being created, this time on the left of the coral (fig 45, bottom plots). There is a large area of higher concentration almost 1 meter high in the middle of this new shadow zone.

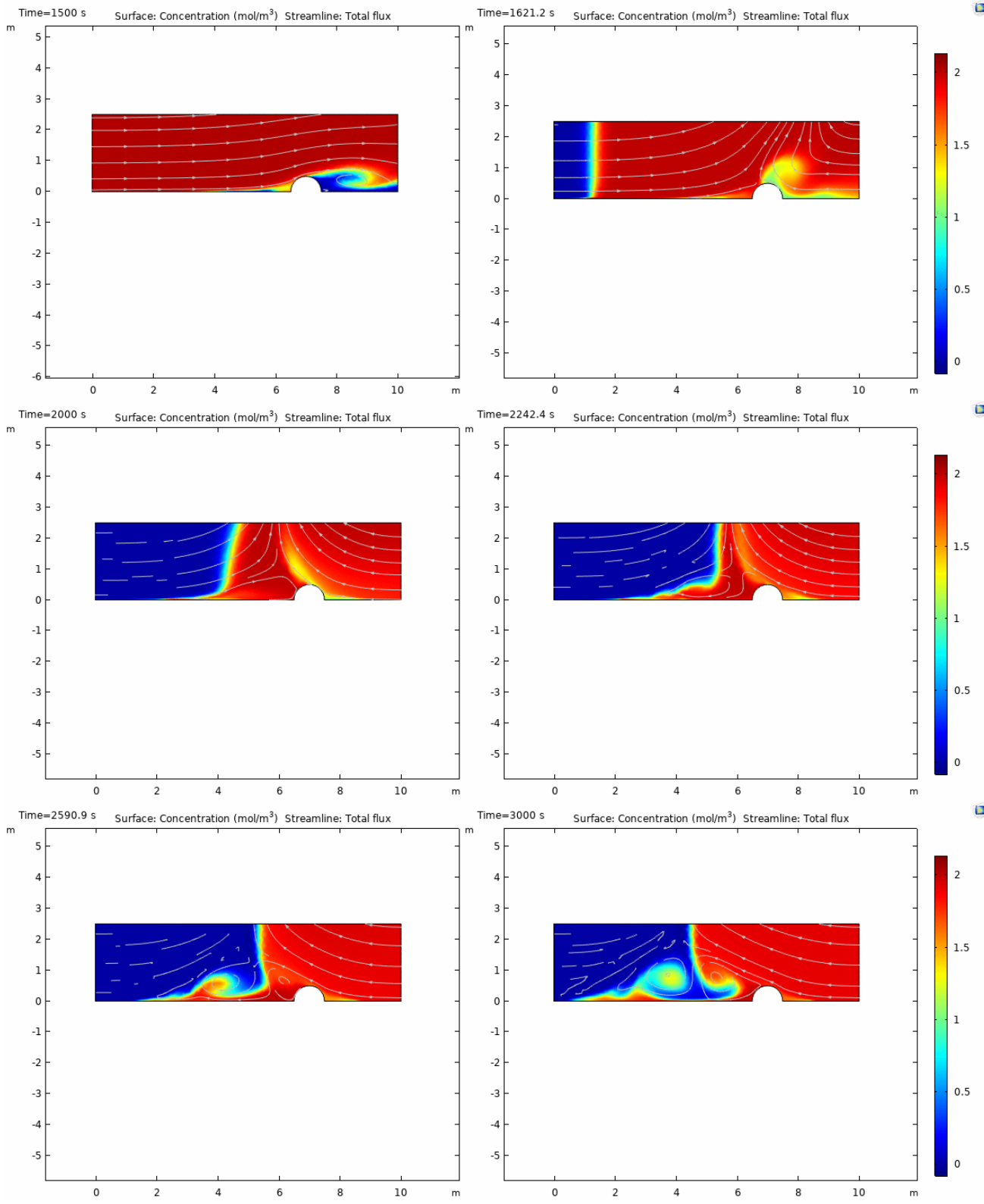


Figure 45: Concentration over time. Solid lines are from a point to the left of the coral, marked lines are from a point to the right. The first 1500 seconds was during normal flow, and the last 1500 seconds was during reverse flow

Figure 46 shows the concentration change over the full time series, at a point to the left and right of the coral, both at .5 m depth. The concentration change seen in the simulation plots on the previous page is very apparent, with the solid lines marking the point to the left of the coral and the marked lines to the right of the coral. The destruction of the shadow zone to the right of the coral is clear in the marked lines, with the sudden increase after time 1500 s, while the formation of the new shadow zone to the left of the coral is seen in the solid lines starting around time 2400 s.

This simulation shows the impact of velocity on the movement of oxygen, and further shows that velocity does have an impact, even though it may not be the only parameter influencing the patterns of oxygen concentration. The implications of this will be further discussed in the next section.

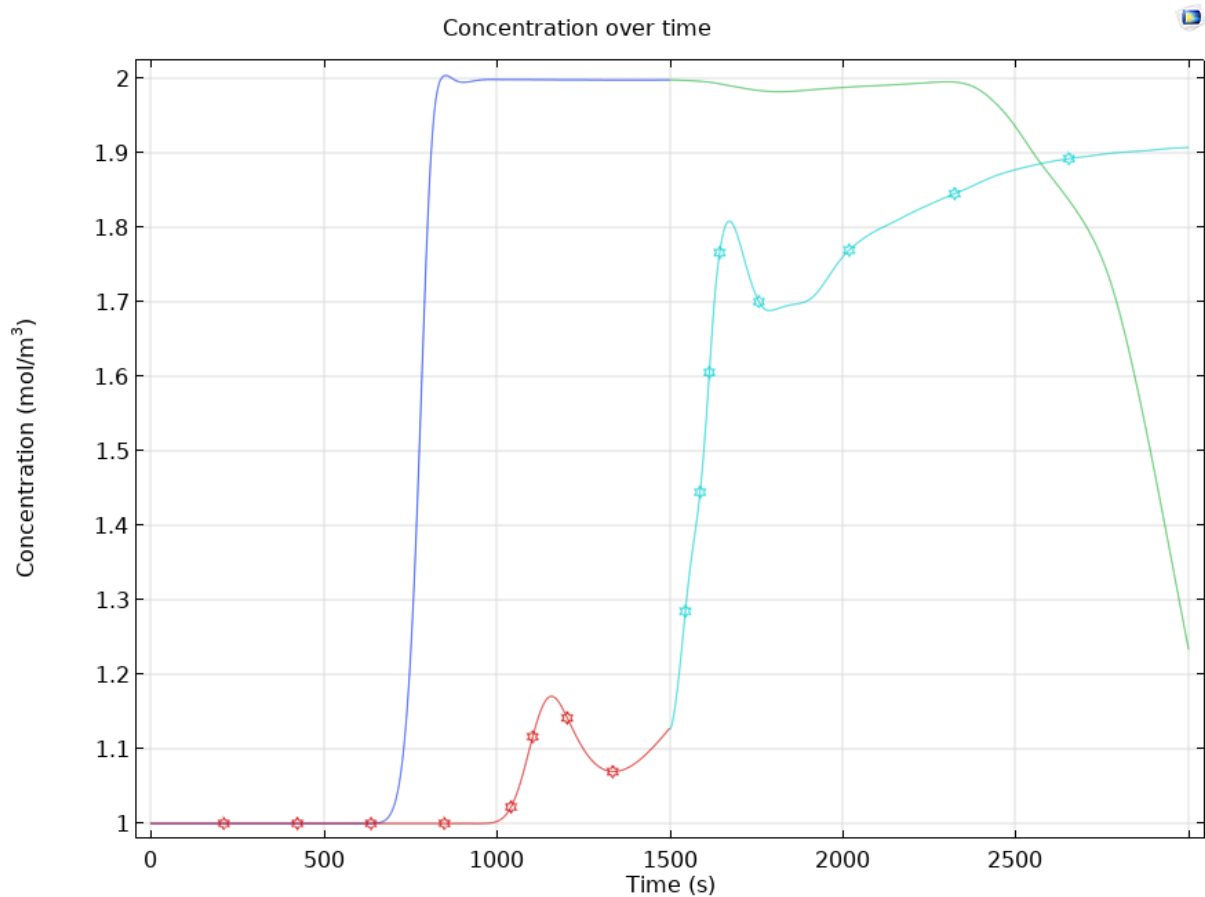


Figure 46: Concentration over time, with a directional switch in velocity. The velocity switched direction at time 1500 s, seen in the color change of each line. The solid lines are from the left side of the coral and the marked lines are from the right side.

## 5. Discussion and future research

This study was focused on the relationship between hydrodynamics and dissolved oxygen around coral reefs in Curaçao. The results of this study provide the SEALINK project insights into previously-unknown information on hydrodynamics and dissolved oxygen movement, and help focus further research. In all study locations, there does appear to be a connection between dissolved oxygen and hydrodynamics, however the extent of that relationship is dependent on the location, tidal cycle (neap or spring tide), and other coastal and meteorological processes that were not in scope for this project.

### 5.1 RQ 1: Are waves and currents measurably different around the island?

The current velocities and wave data were extremely dependent on the locations where they were taken, as well as the tidal cycle. The current speeds and directions of each location (fig 24) showed this very clearly. The biggest differences were seen at Boca Sami and Daaibooi, and East Point was the most unique site. The peak current velocities seen at Boca Sami beach and Daaibooi beach (located north of Boca Sami) are very different, with faster current velocities seen at Boca Sami. The primary direction of flow at Boca Sami is in the north and northwest direction, primarily away from the shore, whereas current at Daaibooi flows primarily north and south-southeast. This is possibly due to local wind patterns, the geography of the beaches, and coral structures at the study sites. Where Boca Sami faces southwest with no land protection towards the south of this location, Daaibooi is surrounded by cliffs and the reefs start at the edge of the cliffs. This difference can also be seen in the velocity data from March 23 (Daaibooi) and March 30 (Boca Sami). Daaibooi is in such a narrow location, and the AD2CP data showed short, sudden changes in direction of velocity, from north to south. This was not seen in the Boca Sami data or at any of the other sites. The data from Boca Sami showed a consistent northward flow, with one long period of increasing flow. The reason for this could be that the current and tides flowing from the beach at Daaibooi are interacting, causing a sudden switch in direction. Both sets of data from Boca Sami also showed the currents switching direction, however only once during the measurement time. This difference in locations could also be due to wind exposure and the resulting surface waves. The surface waves at Daaibooi were often rougher, coming from the south. This in combination with very few coral structures at the study site could be the reason for stronger velocities seen throughout the full depth of the water column. The data from East

Point is rather unique, possibly due to the location and reef orientation. The reef here was most abundant out of all the sites, with a relatively straight coastline. There is no land to the south that protects the reefs or deflects the currents, and the waves were the largest and most frequent here, likely due to the wind. When the tidal signal is taken out of the current flow data (fig 26), it is clear that the tides are a vital part of what determines the speed and direction of currents and waves. The residual flow is being driven by something else, possibly local winds, water density gradients, or changes in sea level. These could all explain the differences seen in figures 25 and 26.

Cleaning and validating some of the data sets in some of the locations (Directors Bay March 13th, AD2CP2; Kalki March 21<sup>st</sup>, AD2CP2; Piscadera Bay March 25<sup>th</sup>), resulted in data too short to be meaningfully compared to the other data sets. This caused some of the AD2CP data sets at the same sites to be of different lengths, and made it difficult to compare them at times. One of our data sets was unusable because the instruments were moved to the shore halfway through the measurement period without our knowledge. There were other instances when the AD2CPs were too shallow and the data was unusable.

## 5.2 RQ 2: Can the found differences in waves and currents be used to predict the level of dissolved oxygen near coral reefs?

The results discussed above can be used to predict the dissolved oxygen concentration only in very specific instances. When the Granger causality test was run on all sites (fig 27 and fig 28), only a few specific dates and locations showed that velocity could be used as a predictor of DO values. It was also very dependent on the location of the AD2CPs and DO loggers. Only the north and east velocities from .95 m above the sea floor were used in this test, and it may be valuable to use the full velocity depth profile and run further causality tests in order to understand this relationship more fully. Velocities throughout the water column could have an influence on the bottom velocities, and therefore could potentially be better predictors of DO concentration. The lack of causality in most of the study locations means that there are other drivers of DO concentration that need to be studied in order to understand the true influence of DO on coral reefs.

As explained before, the Granger causality test only works with stationary time series (i.e. de-trended), and non-stationary time series must be transformed. Even after transformation,

some of the time series used were still not stationary and therefore couldn't be utilized in this statistical method. This method seems to work better with longer time series, and could also be tested with other parameters such as wave height or water pressure. Exploring and testing other statistical analyses was not in the scope of this project, but could be useful in the future.

### 5.3 RQ 3: What can numerical models teach us about the impact of water flow on dissolved oxygen fluctuations?

A modelled simulation with data from the field is a valuable way to understand some of the processes that are responsible for the oxygen values that seen in in-situ data. This was the first time that field velocity values from Curaçao were used in a time-dependent modelled simulation for the SEALINK project. The results of the model give more insight into some of the processes that affect oxygen concentration and dispersal near coral reefs. The simulations show that a changing velocity, both in speed and direction, do have an impact on oxygen concentration, but that alone is not enough to result in some of the patterns seen in the in-situ data. In the model, diffusion, in conjunction with velocity, appears to be a driving factor in oxygen dispersal, as seen in all simulations despite a changing velocity. Although stark changes in diffusion and viscosity aren't seen in a natural environment like simulated in the model, it gives insight into how the processes could affect oxygen concentration patterns, and opens the door for further research. The final simulation showed that a change in flow direction also has an impact on oxygen concentration, and can potentially disrupt shadow zones of low to no oxygen near corals. Understanding that these processes could have an impact on the balance of oxygen in coral reef systems is critical to understanding influences on reef health. This is the first step towards understanding their potential influence and why it occurs.

Given in-situ data, this numerical model is a good way to help reflect on smaller processes and feedbacks happening in the environment that might be responsible for changes in oxygen concentration over time. While this model assists in comprehending simple 2D flow around coral and its influence on oxygen distribution, the model results cannot be directly compared to the field data. This is because the shape of the sea floor, time, and a wind component, among other things, were not incorporated into this model due to the time frame of this thesis. There was no concentration flux applied to the coral in order to simulate the respiration or consumption of oxygen, as is seen in a natural environment. The model is also a laminar flow model, meaning that the flow is fairly calm

and streamlined, however, flow in the ocean around coral reefs can be very turbulent, i.e. rough and disordered. Running a model with turbulent flow would allow for a more realistic water flow and movement of oxygen.

#### 5.4 Future research

Given the limits of this project, there is a lot of work that can be done to improve the models. To further test the functionality and capability of these models, tidal cycles must to be taken into account, as well as data from all measurement days, sites and velocity depth profiles. Because the data used in this model was only from one part of the velocity-depth profile for one day, the modelled parameters that were explored were consequently limited. Expanding the data sets could help to gain a larger picture of the smaller process reasoned about above. Future iterations of the models created would benefit from incorporating more realistic configurations, such as shapes that act as sponges and consume oxygen as it moves through time, different coral orientations in space, different shaped sea bottoms, and, eventually, a 3D component. Providing more realistic boundary conditions and combining these models with larger scale hydrodynamics models, and including tracking of individual oxygen particles could improve the functionality of these models. Creating and working with 2D models that represent a 3D environment is extremely difficult, because 2D models are very conservative in what inputs they can have and what outputs they can give.

Next steps for this research could be to look into how dissolved oxygen moves on a smaller scale around coral reefs, at the boundary layer for instance, and what other factors can influence DO concentrations in natural environments. A better source of the local wind patterns and speeds would be useful in the continued study of waves and currents around Curaçao.

## References

- Alice in wonderland dive site. PADI Travel. (n.d.). Retrieved June 26, 2022, from <https://www.padi.com/dive-site/curacao/playa-kalki/#overview>
- Asher, S., S. Niewerth, K. Koll, & U. Shavit (2016), Vertical variations of coral reef drag forces, *J. Geophys. Res. Oceans*, 121, 3549–3563, doi:10.1002/2015JC011428.
- Badgley, B.D., Lipschultz, F. & Sebens, K.P. (2006). Nitrate uptake by the reef coral *Diploria strigosa*: effects of concentration, water flow, and irradiance. *Marine Biology* **149**, 327–338. <https://doi.org/10.1007/s00227-005-0180-5>
- Barnett, L. & Seth, A. K. (2014). The MVGC multivariate Granger causality toolbox: a new approach to Granger-causal inference. *Journal of neuroscience methods*, 223, 50–68. <https://doi.org/10.1016/j.jneumeth.2013.10.018>
- Becker J, Merrifield M, Ford M. (2014). Water level effects on breaking wave setup for Pacific Island fringing reefs. *J. Geophys. Res.* 119:914–32
- Boca Sami - Sint Michiel: Curaçao Diving Guide: Dive Travel Curacao. (2022, April 04). Retrieved June 26, 2022, from <https://www.divecuracao.info/curacao-dive-travel-guide/curacao-diving-guide/dive-and-snorkel-guide/boca-sami/>
- Bouderlique, T., Petersen, J., Faure, L., Abed-Navandi, D., Bouchnita, A., Mueller, B., ... & Adameyko, I. (2022). Surface flow for colonial integration in reef-building corals. *Current Biology*. <https://doi.org/10.1016/j.cub.2022.04.054>
- Calhoun, S. K., Haas, A. F., Takeshita, Y., Johnson, M. D., Fox, M. D., Kelly, E. L., ... & Smith, J. E. (2017). Exploring the occurrence of and explanations for nighttime spikes in dissolved oxygen across coral reef environments. *PeerJ Preprints*, 5, e2935v2.
- Cordier, E., Lézé, J., & Join, J. (2013). Natural tidal processes modified by the existence of Fringing Reef on La Reunion Island (Western Indian Ocean): Impact on the relative sea level variations. *Continental Shelf Research*, 55, 119-128. doi:10.1016/j.csr.2013.01.016
- Crabbe, M. J., Martinez, E., Garcia, C., Chub, J., Castro, L., & Guy, J. (2008). Growth modelling indicates hurricanes and severe storms are linked to low coral recruitment in the Caribbean. *Marine Environmental Research*, 65(4), 364-368. doi:10.1016/j.marenvres.2007.11.006

de Bakker DM, Meesters EH, Bak RPM, Nieuwland G, Van Duyl FC (2016) Long-term shifts in coral communities on shallow to deep reef slopes of Curaçao and Bonaire: are there any winners? *Frontiers in Marine Science*, 3: 247

De'ath G, Fabricius KE, Sweatman H, Puotinen M. (2012). The 27-year decline of coral cover on the Great Barrier Reef and its causes. *Proc. Natl. Acad. Sci. USA* 109:17995–99

Directors bay caracasbaai: Curacao Diving Guide: Dive Travel Curacao. (2022, April 10). Retrieved June 26, 2022, from <https://www.divecuracao.info/curacao-dive-travel-guide/curacao-diving-guide/dive-and-snorkel-guide/directors-bay/>

Eastpoint Curacao: Curaçao Diving Guide: Dive Travel Curacao. (2022, April 04). Retrieved June 26, 2022, from <https://www.divecuracao.info/curacao-dive-travel-guide/curacao-diving-guide/dive-and-snorkel-guide/eastpoint/>

Finelli, C. M., Helmuth, B. S., Pentcheff, N. D., & Wethey, D. S. (2006). Water flow influences oxygen transport and photosynthetic efficiency in corals. *Coral Reefs*, 25(1), 47-57.

Gardella, D. J., & Edmunds, P. J. (1999). The oxygen microenvironment adjacent to the tissue of the scleractinian *Dichocoenia stokesii* and its effects on symbiont metabolism. *Marine Biology*, 135(2), 289-295.

Granger, C. W. (1969). Investigating causal relations by econometric models and cross-spectral methods. *Econometrica: journal of the Econometric Society*, 424-438.

Green, R. H., Lowe, R. J., & Buckley, M. L. (2018). Hydrodynamics of a tidally forced coral reef atoll. *Journal of Geophysical Research: Oceans*, 123, 7084–7101. <https://doi.org/10.1029/2018JC013946>

Guerra, M., & Thomson, J. (2017). Turbulence measurements from five-beam acoustic Doppler current profilers. *Journal of Atmospheric and Oceanic Technology*, 34(6), 1267–1284. <https://doi.org/10.1175/jtech-d-16-0148.1>

Haas AF, Gregg AK, Smith JE, Abieri ML, Hatay M, Rohwer F. 2013. Visualization of oxygen distribution patterns caused by coral and algae. *PeerJ* 1:e106 <https://doi.org/10.7717/peerj.106>

Harriot, V.J. (1999) Coral growth in subtropical eastern Australia. *Coral Reefs* Vol 18. pgs 281-291

Hill, A. E. (1991). Vertical migration in tidal currents. *Marine ecology progress series. Oldendorf*, 75(1), 39-54.

Jackson-Bue, T., Williams, G. J., Whitton, T. A., Roberts, M. J., Brown, A. G., Amir, H., ... & Davies, A. J. (2022). Seabed morphology and bed shear stress predict temperate reef habitats in a high energy marine region. *Estuarine, Coastal and Shelf Science*, 107934.

- Kühl, M., Cohen, Y., Dalsgaard, T., Jørgensen, B. B., & Revsbech, N. P. (1995). Microenvironment and photosynthesis of zooxanthellae in scleractinian corals studied with microsensors for O<sub>2</sub>, pH and light. *Marine Ecology-Progress Series*, 117(1-3), 159-172.
- Leichter, J. J., Deane, G. B., & Stokes, M. D. (2005). Spatial and temporal variability of internal wave forcing on a coral reef. *Journal of Physical Oceanography*, 35(11), 1945-1962.
- Li, S. (n.d.). *Machine-learning-with-python/granger causality test.ipynb at master · susanli2016/machine-learning-with-python*. GitHub. Retrieved June 30, 2022, from <https://github.com/susanli2016/Machine-Learning-with-Python/blob/master/Granger%20Causality%20Test.ipynb>
- Lowe, R. J., Koseff, J. R., & Monismith, S. G. (2005). Oscillatory flow through submerged canopies: 1. Velocity structure. *Journal of Geophysical Research*, 110, C10016. <https://doi.org/10.1029/2004JC002788>
- Lowe, R. J., Shavit, U., Falter, J. L., Koseff, J. R., & Monismith, S. G. (2008). Modeling flow in coral communities with and without waves: A synthesis of porous media and canopy flow approaches. *Limnology and Oceanography*, 53(6), 2668–2680. <https://doi.org/10.1029/2004JC002788>
- Marine Scientific Assessment (2017). *The State of Curaçao's Coral Reefs*. Waitt Institute. [https://www.waittinstitute.org/files/ugd/47d1fd\\_b3e7537b9084480cbe31034de70ed7b8.pdf](https://www.waittinstitute.org/files/ugd/47d1fd_b3e7537b9084480cbe31034de70ed7b8.pdf)
- Mass, T., Genin, A., Shavit, U., Grinstein, M., & Tchernov, D. (2010). Flow enhances photosynthesis in marine benthic autotrophs by increasing the efflux of oxygen from the organism to the water. *Proceedings of the National Academy of Sciences*, 107(6), 2527-2531.
- McCook L, Jompa J, Diaz-Pulido G (2001) Competition between corals and algae on coral reefs: a review of evidence and mechanisms. *Coral Reefs* 19(4): 400-417
- Meteorological department curacao*. Meteorological Department Curacao. (n.d.). Retrieved June 26, 2022, from <https://www.meteo.cw/>
- Monismith, S. G. (2007). Hydrodynamics of coral reefs. *Annu. Rev. Fluid Mech.*, 39, 37-55.
- Mosedale, T. J., Stephenson, D. B., Collins, M., & Mills, T. C. (2006). Granger causality of coupled climate processes: Ocean feedback on the North Atlantic Oscillation. *Journal of climate*, 19(7), 1182-1194.
- Nelson, H. R., & Altieri, A. H. (2019). Oxygen: the universal currency on coral reefs. *Coral Reefs*, 38(2), 177-198.
- Nortek. (2022) *Principles of Operation*. Nortek Manuals. <https://support.nortekgroup.com/hc/en-us/articles/360029835831-Principles-of-Operation-Signature>

NWO. (2021). *Land, sea, and society: Linking terrestrial pollutants and inputs to nearshore coral reef growth to identify novel conservation options for the Dutch Caribbean (Sealink)*. NWO. Retrieved June 30, 2022, from <https://www.nwo.nl/projecten/nwoca2019003>

Reidenbach, M. A., Koseff, J. R., Monismith, S. G., Steinbuckc, J. V., & Genin, A. (2006). The effects of waves and morphology on mass transfer within branched reef corals. *Limnology and Oceanography*, *51*(2), 1134-1141.

Sandin, Stuart A., Sheila M. Walsh, and Jeremy BC Jack- son. "Prey release, trophic cascades, and phase shifts in tropical nearshore ecosystems."Trophic cascades: pred- ators, prey, and the changing dynamics of nature(2010): 71-90.

*Seawater - properties*. Engineering ToolBox. (n.d.). Retrieved June 30, 2022, from [https://www.engineeringtoolbox.com/sea-water-properties-d\\_840.html](https://www.engineeringtoolbox.com/sea-water-properties-d_840.html)

Stocking JB, Laforsch C, Sigl R, Reidenbach , MA (2018). The role of turbulent hydrodynamics and surface morphology on heat and mass transfer in corals. *J. R. Soc. Interface* *15*: 20180448. <http://dx.doi.org/10.1098/rsif.2018.0448>

The SEALINK Project. Sealink. (2021). Retrieved June 26, 2022, from <https://www.sealinkcaribbean.net/>

Tirabassi, G., Masoller, C., & Barreiro, M. (2015). A study of the air–sea interaction in the South Atlantic Convergence Zone through Granger causality. *International Journal of Climatology*, *35*(12), 3440-3453

US Department of Commerce, N. (2014). Why do we have spring tides in the fall? Retrieved June 26, 2022, from <https://oceanservice.noaa.gov/facts/springtide.html>

Van Rooijen, A., Lowe, R., Rijnsdorp, D., Ghisalberti, M., Jacobsen, N. G., & McCall, R. (2020). Wave-driven mean flow dynamics in submerged canopies. *Journal of Geophysical Research: Oceans*, *125*, e2019JC015935. <https://doi.org/10.1029/2019JC015935>

Vermeij MJA, Debrot AO, van der Hal N, Bakker J, Bak RP (2010) Increased recruitment rates indicate recovering populations of the sea urchin diadema antillarum on Curacao. *Bulletin of Marine Science* 86:719-725

Veron, J.E.N. (2000a). *Corals of the World*. Townsville: Australian Institute of Marine Science. Volumes 1-3. 1410pp.



## Appendix A – AD2CP Deployment Plans

	Plan A: Alternating			Plan B: Alternating			Plan C: Concurrent		
	Average	Burst	Waves	Average	Burst	Waves	Average	Burst	Waves
<i>Profile Start (m)</i>	.2	.1	6.2	.2	.1	4.8	.2	.1	n/a
<i>Profile End (m)</i>	13	10	13	10	10	10	10	10	n/a
<i>Cell Size (m)</i>	.5	.5	.6	.5	.5	.5	.5	.8	n/a
<i>Average Time Interval</i>	00:02:00	n/a	n/a	00:02:00	n/a	n/a	00:02:00	n/a	n/a
<i>Measurement Interval</i>	00:10:00	00:30:00	02:30:00	00:10:00	00:30:00	02:30:00	00:10:00	01:00:00	n/a
<i>Sampling Rate (Hz)</i>	n/a	8	2	n/a	8	4	n/a	4	n/a
<i>Sample Size</i>	n/a	2048	2048	n/a	4096	4096	n/a	4069	n/a
<i>Burst Duration</i>	n/a	00:04:16	00:17:04	n/a	00:08:32	00:17:04	n/a	00:16:57	n/a
<i>Number of Beams</i>	4	1	4	4	1	4	4	5	n/a

**Plan D: Concurrent**                      **Plan E: Single**                      **Plan F: Concurrent**

	Average	Burst	Waves	Average	Burst	Waves	Average	Burst	Waves
<i>Profile Start (m)</i>	.2	n/a	4.8	n/a	.1	n/a	.2	.1	n/a
<i>Profile End (m)</i>	10	n/a	10	n/a	10	n/a	10	10	n/a
<i>Cell Size (m)</i>	.5	n/a	.5	n/a	1	n/a	.5	1	n/a
<i>Average Time Interval</i>	00:02:00	n/a	n/a	n/a	n/a	n/a	00:02:00	n/a	n/a
<i>Measurement Interval</i>	00:10:00	n/a	00:02:30	n/a	00:30:00	n/a	00:10:00	00:30:00	n/a
<i>Sampling Rate (Hz)</i>	n/a	n/a	4	n/a	8	n/a	n/a	4	n/a
<i>Sample Size</i>	n/a	n/a	4096	n/a	4069	n/a	n/a	3600	n/a
<i>Burst Duration</i>	n/a	n/a	00:17:04	n/a	00:08:28	n/a	n/a	00:15:00	n/a
<i>Number of Beams</i>	4	n/a	4	n/a	5	n/a	4	5	n/a

	Plan G: Concurrent				Plan H: Concurrent				Plan I: Concurrent			
	Average	Burst	Waves	Average	Burst	Waves	Average	Burst	Waves	Average	Burst	Waves
<i>Profile Start (m)</i>	.2	.1	n/a	.2	n/a	4.8	.2	.1	n/a	.2	.1	n/a
<i>Profile End (m)</i>	8	8	n/a	10	n/a	10	10	10	10	10	10	n/a
<i>Cell Size (m)</i>	1	1	n/a	.5	n/a	.5	.5	1	n/a	.5	1	n/a
<i>Average Time Interval</i>	00:02:00	n/a	n/a	00:02:00	n/a	n/a	00:02:00	n/a	n/a	00:02:00	n/a	n/a
<i>Measurement Interval</i>	00:10:00	00:30:00	n/a	00:10:00	n/a	00:30:00	00:10:00	00:30:00	n/a	00:10:00	00:30:00	n/a
<i>Sampling Rate (Hz)</i>	n/a	4	n/a	n/a	n/a	4	n/a	4	n/a	n/a	4	n/a
<i>Sample Size</i>	n/a	3600	n/a	n/a	n/a	7200	n/a	3600	n/a	n/a	3600	n/a
<i>Burst Duration</i>	n/a	00:15:00	n/a	n/a	n/a	00:30:00	n/a	00:15:00	n/a	n/a	00:15:00	n/a
<i>Number of Beams</i>	4	5	n/a	4	n/a	4	4	5	n/a	4	5	n/a

**Plan J:  
Concurrent**

**Plan K:  
Concurrent**

	Average	Burst	Waves	Average	Burst	Waves
<i>Profile Start (m)</i>	.2	.1	n/a	.2	n/a	2.6
<i>Profile End (m)</i>	8	8	n/a	6	n/a	6
<i>Cell Size (m)</i>	.5	1	n/a	.5	n/a	.5
<i>Average Time Interval</i>	00:02:00	n/a	n/a	00:02:00	n/a	n/a
<i>Measurement Interval</i>	00:10:00	00:30:00	n/a	00:10:00	n/a	00:30:00
<i>Sampling Rate (Hz)</i>	n/a	4	n/a	n/a	n/a	2
<i>Sample Size</i>	n/a	3600	n/a	n/a	n/a	3600
<i>Burst Duration (time)</i>	n/a	00:15:00	n/a	n/a	n/a	00:30:00
<i>Number of Beams</i>	4	5	n/a	4	n/a	4

## Appendix B – Model metadata

<b>LAMINAR FLOW</b>	
<i>INLET:STATIONARY</i>	.04 m/s
<i>INLET: FINAL</i>	.01 m/s
<i>SIMULATION</i>	
<b>TRANSPORT OF DILUTED SPECIES</b>	
<i>INITIAL CONCENTRATION</i>	1
<i>INFLOW: CONSTRAINED CONCENTRATION</i>	2
<i>OPEN BOUNDARY</i>	1
<b>SIMULATIONS</b>	
<i>S1</i>	
<i>DIFFUSION</i>	9 e-8 m <sup>2</sup> /s
<i>VISCOSITY</i>	1 e-3 Pa*s
<i>S2</i>	
<i>DIFFUSION</i>	9 e-8 m <sup>2</sup> /s
<i>VISCOSITY</i>	9 e-4 Pa*s
<i>S3</i>	
<i>DIFFUSION</i>	9 e-8 m <sup>2</sup> /s
<i>VISCOSITY</i>	9 e-4 Pa*s
<i>S4</i>	
<i>DIFFUSION</i>	2 e-4 m <sup>2</sup> /s
<i>VISCOSITY</i>	9 e-4 Pa*s
<i>FINAL</i>	
<i>DIFFUSION</i>	9 e-8 m <sup>2</sup> /s
<i>VISCOSITY</i>	9 e-4 Pa*s

Table 2: Model parameters for all simulations

## Appendix B.1 – Time-interpolated velocity

<b>TIME (S)</b>	<b>VELOCITY (M/S)</b>
<b>0</b>	.01
<b>30</b>	0.011
<b>60</b>	0.013
<b>90</b>	0.015
<b>120</b>	0.017
<b>150</b>	0.017
<b>180</b>	0.018
<b>210</b>	0.019
<b>240</b>	0.017
<b>270</b>	0.020
<b>300</b>	0.022
<b>330</b>	0.025
<b>360</b>	0.030
<b>390</b>	0.032
<b>420</b>	0.034
<b>450</b>	0.034
<b>480</b>	0.035
<b>510</b>	0.037
<b>540</b>	0.039
<b>570</b>	0.040
<b>600</b>	0.044
<b>630</b>	0.046
<b>660</b>	0.046
<b>690</b>	0.047
<b>720</b>	0.045
<b>750</b>	0.042
<b>780</b>	0.043

*Table 3: Velocity values from Boca Sami on March 8th over time. The values were used in an interpolation function as inlet values for S1-S4.*

## Acknowledgements

The focus of this thesis was on the relationship between hydrodynamics, specifically currents and waves, and dissolved oxygen concentration near coral reefs around the island of Curaçao. It was conducted as part of the finalization of the Master of Marine Science at Utrecht University. This project was supervised by the Royal Netherlands Institute for Sea Research (NIOZ), and guided by supervisors Paolo Stocchi, Vesna Bertoneclj (PhD candidate), Andi Haas, and Jack Middelburg (Utrecht University). There is a long list of people that I'd like to thank that helped make this project a reality:

First, to all of the people that are part of the SEALINK project: thank you for welcoming me with open arms and making me feel like a part of the team from day one! Your encouragement and excitement about my project kept me going in tough times, and you all gave great advice. Your passion for all that you do is inspiring.

Second, to the PhD student that got stuck with me for the entirety of our field work, Vesna Bertoneclj. Thank you for entertaining my sometimes wild and crazy ideas for fieldwork, and being so willing to work as hard as possible in occasionally extreme conditions. Thank you also for letting me pick your brain for ideas for my thesis paper, for the great advice you gave, and for being the best dive buddy I could have hoped for.

Third, thank you to all the other people at NIOZ that have assisted with parts of this project: Andi Haas, for being my third supervisor and lending me equipment to use for fieldwork! I could not have succeeded in this project without your assistance and awesome ideas. Thank you to Virginia Sanchez for helping determine study locations, assisting with some data analysis, and always being up for a coffee chat when I needed it! Thank you to Adam Candy for being the greatest advisor on computational modelling, for providing 3D photomosaics for our locations on Curaçao, and for being so willing to assist me on this project.

Fourth, to the rangers at CARMABI that assisted us in our East Point dives! Thank you for enduring rough waves and bad weather and being so willing to offer your assistance in this project!

Finally, thank you to my family for supporting me through this milestone! Thank you especially to my fiancée, Maya Lacy, for encouraging me to do this in the first place and not

give up on a life-long dream. Thank you also to my future mother-in-law, Laurie Lacy, for having multiple hour-long conversations with me about this paper when I needed guidance.